UCLouvain

FACULTE DES SCIENCES

Faculté des sciences

Construction, characterisation and frequency stabilisation of an External Cavity Diode Laser for future high-precision and high-power studies

Mémoire présenté en vue de l'obtention du grade académique de Master [120] en sciences physiques

Author : Charlotte Bragard

Supervisor : Clément Lauzin

Readers : Matthieu Génévriez and Xavier Urbain

École de Physique

Academic year 2024-2025

Acknowledgement

The completion of this master's thesis would not have been possible without the support and contributions of the entire NAPS team.

I would like to sincerely thank Pr. Clément Lauzin for giving me the opportunity to work on such an engaging topic and for allowing me the flexibility to change the course of my master's thesis during the year.

My gratitude also goes to Ricardo and ALexandr for patiently teaching me how things needed to be done in the lab, for taking the time of answering my many questions, and for helping me with my results analysis.

Thank you to Arthémise, Simon and Alexis for always being available to provide guidance and assistance whenever it was needed.

A special thanks to Guillaume for always being there to listen to me rant about my experiments and the many coffee breaks we shared.

I would also like to thank my family and friends for their constant support, encouragement, and understanding throughout this journey. Their presence, even outside the lab, made all the difference.

Contents

1 Introduction

The concept of time has evolved alongside human's understanding of nature.

In modern physics, the definition of time has been refined and specified using fundamental properties of nature. Today, the International System of Units (SI) defines time based on a physical constant. The base time unit, the second, is defined by the transition frequency of the hyperfine transition of the fundamental state of a cesium 133 atom [1]:

$$\Delta f_{Cs} = 9\ 192\ 631\ 770 \text{ Hz}. \tag{1.1}$$

Therefore, one second is defined as :

$$1\text{s} = \frac{9\ 192\ 631\ 770}{\Delta f_{Cs}}. \tag{1.2}$$

This definition of the second ensures that timekeeping is based on a universal constant, and therefore reaching an unprecedented level of precision. However, it is based on an idealised system where the cesium atom is unperturbed in free space and the observer is in another reference frame than the atom.
In practice, the International Atomic Time (TAI) is generated by coordinated global effort; a worldwide network of laboratories send data from very precise clocks, which are then averaged to produce a global timescale. This timescale is compared afterwards to primary frequency standards, such as hydrogen maser, cesium and rubidium standards, to ensure that the definition of the second remains as close as possible to the SI definition.

Optical clocks are among the most advanced timekeeping devices and are used as reference frequency standards. An optical clock is typically composed of three main components : a frequency reference, an atomic transition or a stable optical cavity mode for example, a measurement system to detect the signal generated by the frequency reference, and a display system to show the output result [2].

Frequency standards are multiple : hydrogen masers, cesium and rubidium standards, as explained before, microwave atomic standard, optical atomic clocks (trapped ion clocks, optical lattice clocks) or even optical cavity modes. These frequency standard are characterised by their frequency stability over time, which is a unitless value, and is used to indicate the accuracy of a frequency measurement given a certain time interval. For example, for simple quartz watches, a study has shown that they reach a stability of around 10^{-8} over one week, which corresponds to a

drift of a few milliseconds per day [3]. For reference, the cesium clock used for timekeeping in the United States has a frequency stability of 10^{-17} per day [4]. As for the hydrogen masers, they exhibit a stability of around 10^{-16} over a few days [5]. Additionally, it has been shown that optical lattice clock using strontium atoms has reached a level of stability of 10^{-17} over 1000 s [6]. For an optical cavity at room temperature, stability below 10^{-16} for long averaging times, up to 10^3 s, has been demonstrated [7].
Building optical clocks with really high level of stability is necessary to confirm time dilation caused by relativistic effects [8, 9].

In this work, we are interested in clocks based on optical cavities. These clocks use a laser locked to a very stable optical cavity as the local oscillator for the clock [10]. This locking allows to narrow significantly the linewidth of the laser, allowing to probe accurately the atomic transition of reference.
Different locking techniques exist and have been used for this purpose. In [11], an ECDL, of initial linewidth of 160 kHz, was side locked to a Fabry-Pérot Interferometer fringe, narrowing it to 400 Hz. The Pound-Drever-Hall (PDH) locking technique has also been proven to efficiently narrow a laser's linewidth, reaching the sub-hertz level. In [12], resonant optical feedback was used to reduce the linewidth of a semiconductor laser from 20 MHz to approximately 20 kHz. In [13], the authors employed a high-finesse cavity and an ECDL for PDH lock, reducing the beatnote linewidth from 175 kHz to 150 Hz. More recently, high-finesse ULE cavities were used to reduce the linewidth of ECDLs to less than 1 Hz [14]. In 2024, S. Peil et al [15] present the progress in optical clock development. They explain that they use a 1542 nm diode laser, stabilised to high-finesse ULE cavity optical oscillator, as an optical oscillator for their clock.

This master's thesis aims to build an optical clock using a narrow-linewidth ECDL and frequency-stabilising it by PDH-lock to a mechanically stable high-finesse optical cavity.

This manuscript is organised as follows. Chapter 2 provides the theoretical concepts needed to understand this project, covering the principles behind the ECDL, the PDH-locking technique, and different methods to characterise optical clocks. Chapter 3 describes the different experimental setups that were developed and used throughout this work. The results obtained with these different setups are presented and discussed in Chapter 4. Finally, Chapter 5 concludes this manuscript and offers perspectives for future improvements.

2 Theory

2.1 External Cavity Diode Laser (ECDL)

An ECDL is a type of tunable laser that is both affordable, customisable, and characterised by a narrow linewidth, typically of a few hundreds of kHz. These characteristics make it a perfect adjustable tool for research applications. As illustrated in Figure 2.1, a classical ECDL in the Littrow configuration is composed of a laser diode, an anti-reflective (AR) coated lens, a grating, a mirror, and a piezoelectric transducer (PZT).

Light emitted from the laser diode passes through the AR-coated lens and is diffracted by the grating. The first-order diffracted beam is reflected back into the diode, forming the external cavity. The relation between the angle at which the light meets the grating θ, the angle of diffraction θ' and the wavelength of the laser λ is :

$$a(\sin\theta + \sin\theta') = \lambda \tag{2.1}$$

with a the grating groove spacing [16].
In the Littrow configuration, to ensure that the diffracted light is reflected back into the laser, the angle of diffraction and the incident angle must be equal, $\theta = \theta'$. Equation 2.1 can therefore be rewritten as :

$$\sin\theta = \frac{\lambda}{2a} \tag{2.2}$$

When a non-AR-coated laser diode is used, an internal cavity is formed between the diode's front and the back facets. The consequence of this internal cavity is a mode competition between the internal and the external cavities. This mode competition

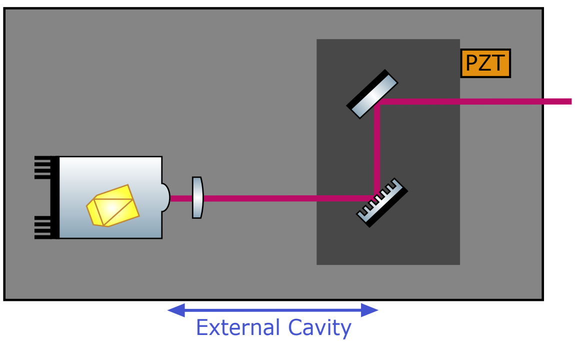

Figure 2.1: Littrow configuration of an External Cavity Diode Laser, adapted from [16].

causes a wide range of output frequencies. The laser ultimately operates at the frequency corresponding to the mode with the highest gain, represented by the red box in Figure 2.2.

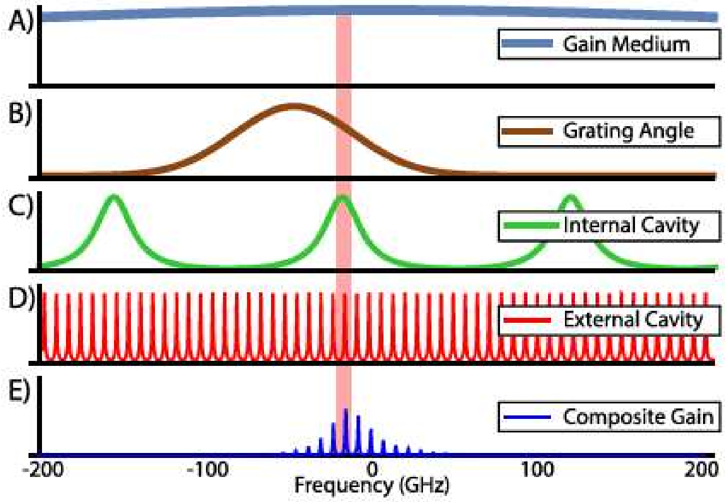

Figure 2.2: ECDL laser frequency selection for non-AR-coated diode laser, from [16].

The tuning of the ECDL's output frequency can be achieved in three different ways : adjusting the grating angle, modifying the length of the external cavity, or changing the laser diode current. These tuning techniques need to be done in parallel to avoid any mode hopping.

- Grating angle tuning.

  From Equation 2.2, the frequency tuning due to the adjusting of the grating angle can be expressed as :

$$\frac{df}{d\theta} = -\frac{2ac}{\lambda^2}\cos\theta, \tag{2.3}$$

  where the expression of $df/d\theta$ was developed using :

$$\frac{d\lambda}{d\theta} = \frac{df}{d\theta}\frac{d\lambda}{df} = \frac{df}{d\theta}\left(-\frac{c}{f^2}\right) \implies \frac{df}{d\theta} = -\frac{f^2}{c}\frac{d\lambda}{d\theta}$$

- Cavity length tuning.

  Changing the length, l, of the external cavity will impose a frequency shift of the resonant frequency of a cavity mode by:

$$\frac{\delta f}{f} = -\frac{\delta l}{l}.$$

  Consequently, the frequency shift caused by the cavity length tuning is described as :

$$\frac{df}{dl} = -\frac{c}{\lambda l} \tag{2.4}$$

- Laser diode current tuning.

  The cavity of a laser diode is a p-n junction within in a Fabry-Pérot (FP) resonator. The p-n junction is forward biased, and when a current is applied to the diode laser, light is generated through population inversion. The presence of the FP reflecting surfaces will allow the stimulated emission and the optical feedback needed in a laser. Modifying the current will change the dimensions of the recombination zone, which in turn will modify the output laser frequency.

These multiple methods of frequency tuning are what makes ECDLs a powerful tool in optical metrology and precision spectroscopy.

Since the 1980s, numerous studies have reported on the assembly of ECDLS, operating between 600 nm and 1550 nm, with linewidths ranging from below 10 kHz to 100 kHz, and with mode hop-free tuning ranges up to 200 nm [17–22]

2.2 Pound-Drever-Hall method

The Pound-Drever-Hall (PDH) method [23] is a technique used to precisely lock a laser to an optical cavity, or conversely, to lock an optical cavity to a laser. This technique allows to stabilise precisely the laser frequency relative to the frequency stability of the cavity.

In this method, the laser beam is phase modulated using an electro-optic modulator (EOM) (or an acousto-optic modulator (AOM) [24]) before being sent to a cavity. The laser beam has an initial electric field given by : $E_i(t) = E_0 e^{i\omega_c}t$, with E_0 the amplitude of the field and ω_c its angular frequency. After being phase modulated at a frequency ω_m, the laser field consists of three spectral components, the carrier at ω_c, and two sidebands at $\omega_c \pm \omega_m$:

$$E(t) = E_0\, e^{i\omega_c t}\left[1 + \frac{\beta}{2}\, e^{i\omega_m t} - \frac{\beta}{2}\, e^{-i\omega_m t}\right], \tag{2.5}$$

with $\beta < 1$ the modulation index. These three spectral components are referred to as the frequency modulated triplet. Note that the two sidebands are 180° out of phase from each other. The laser frequency should then be tuned so that the carrier of the FM triplet is in resonance with a cavity mode.

To monitor the locking process, the light reflected from the cavity's input mirror is sent into a photodiode. The detected signal in reflection is composed of the interference between the reflected light directly from the mirror and some light leaking from the optical cavity.

A schematic representation of a typical PDH experimental setup is shown in Figure 2.3. The signal from the photodiode in reflection is mixed with the signal from the local oscillator driving the EOM at a frequency ω_m. A phase shifter is placed between the oscillator and the mixer to compensate for time delays in the two different signal paths. After the mixer, the signal goes through a low pass filter to isolate the DC frequency signal. These components form the feedback loop that adjusts the laser frequency, keeping it in resonance with the cavity mode.

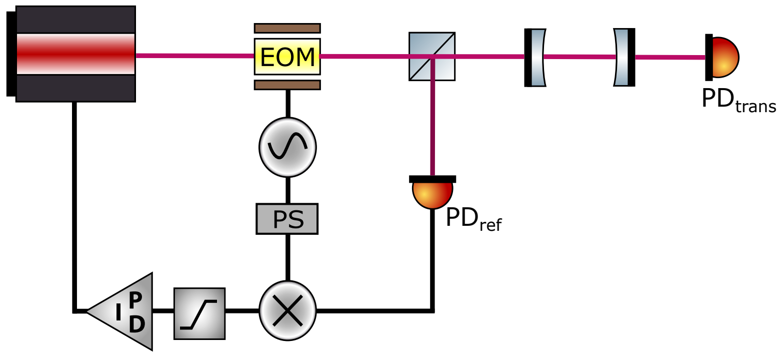

Figure 2.3: Example of the layout of a PDH setup, adapted from [25]. EOM stands for electro-optic modulator, PS stands for phase shifter and PID means Proportional, Integral and Derivative controller.

The signal after the mixer and the low-pass filter is used as the PDH error signal. This error signal depends on the reflected field, and its expression is given by [25]:

$$\epsilon = \sqrt{P_S P_C} \cdot \mathrm{Im}\left[F(\omega)F^*(\omega+\omega_m) - F^*(\omega)F(\omega-\omega_m)\right]; \tag{2.6}$$

where P_S and P_C are the powers of the sidebands and the carrier respectively. The choice of modulation frequency is very critical in a PDH setup. If this frequency is smaller than the cavity mode width, the error signal will not show resolved resonances, as shown in Figure 2.4a. Conversely, selecting a modulation frequency higher than the cavity mode width allows each sidebands to probe the mode individually. The corresponding error signal is shown in Figure 2.4b.
In Equation 2.6, $F(\omega)$ is the cavity reflection coefficient at the frequency ω :

$$F(\omega) = \sqrt{r}\,\frac{1 - e^{i\omega/\nu_{FSR}}}{1 - r\;e^{i\omega/\nu_{FSR}}}, \tag{2.7}$$

with r, the amplitude reflection coefficient and, $\nu_{FSR} = c/2L$, the cavity free spectral range of the optical cavity of length L.

The PDH error signal tends abruptly to zero near the resonances. Indeed, by looking at the mathematical expression of $F(\omega)$, if we use the fact that $\omega = 2\pi\nu$, it is clear that when $\nu = n\nu_{FSR}$, with $n \in \mathbb{Z}$, the reflection coefficient vanishes. Consequently, the reflected power detected by the photodiode drops to zero.
Physically, the error signal tends to zero because when the carrier is in resonance with the cavity mode, it is almost completely transmitted into the cavity. Meanwhile, the sidebands are almost completely reflected from the cavity. Because they are 180° out of phase with each other, their interference is cancelled in the demodulation process, leading to a zero-crossing in the error signal. The laser frequency then drifts away from the resonance and is no longer perfectly coupled into the cavity. The interference between the reflected sidebands and carrier becomes asymmetric, causing a non zero error signal. Importantly, the behaviour of the error

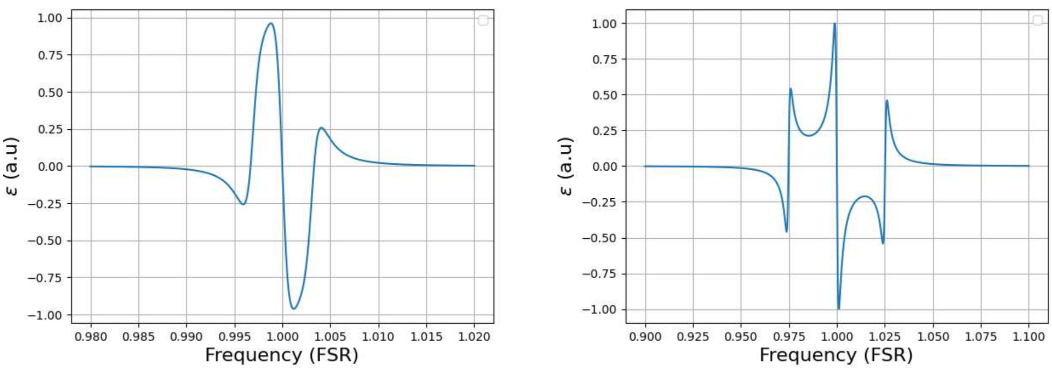

(a) (b)

Figure 2.4: PDH error signal, in terms of the number of FSRs. These error signals were simulated for a cavity finesse of around 500, with a mode width of MHz. The signal in (a) was simulated with a modulation frequency of 1 MHz. The signal in (b) was simulated for a modulation frequency of 8 MHz.

signal around resonance is linear with a very steep slope. This slope is wanted to be as steep as possible so that the probing of the spectral feature of interest is as precise as possible. In practical terms, a small frequency variation $\Delta\nu$ corresponds to a large voltage variation ΔI in the error signal.

In the literature, it has been showed that the stability of the PDH locking technique can reach down to the ppm of the cavity mode linewidth [26, 27].

2.3 Characterisation of optical clocks

In this work, the characterisation of a home-built optical clock is carried out using two different methods. The first method involves the measurement of the ECDL linewidth to have an idea of the frequency precision of the clock. The second method focuses on the different frequency noises present in the system to define its stability over time.

Various type of noises can be defined, depending on their physical origin. Their following description is based on the chapter 2 of [2].
Flicker noise is attributed to the electronic components of the system. This type of noise rises from impurities in a conductive material or generation and recombination noise in a semiconductor under bias. In the frequency domain, the power spectral density associated to the flicker noise follows a $1/f$ law.
White noise is a type of noise that is independent of the frequency, its power spectral density follows a f^0 behaviour [28]. White noise encompasses both *thermal noise* and *shot noise*. *Thermal noise*, or *Johnson-Nyquist noise*, is due to the thermal agitation of charge carriers inside a conductive material for example. *Shot noise* is caused by the quantisation of photons, for an optical system, or the electric charge carried by electrons in an electronic system. It is impossible to predict the motion of individual particles but their average velocity can be computed. The variation around this average velocity is then called the shot noise [2].

Random walk noise, or **Brownian noise**, is caused by environmental influences, like temperature or vibrations [29], and has a power spectral density with $1/f^2$ behaviour. For example, *thermodynamic noise* is a type of Brownian noise, as it is caused by the thermal exchange between the system and its environment.

2.3.1 Laser linewidth determination

To determine the ECDL linewidth, a stabilised optical frequency comb is used as a frequency reference.

A frequency comb is made of a mode-locked pulsed laser that emits extremely short pulses in the time domain, resulting in a broad spectrum in the frequency domain. This pulsed laser operates with a fixed repetition period t_r, which corresponds to a fixed repetition frequency $f_r = 1/t_r$ between each comb tooth in the frequency domain, as illustrated in Figure 2.5. The frequency of the nth tooth of the comb is expressed as :

$$f_n = f_0 + nf_r, \tag{2.8}$$

where f_0 is the carrier envelope offset frequency. This offset frequency is explained by the fact that dispersion is created inside the laser cavity, generating a phase shift $\Delta\phi$ between the envelope of the electric field and the carrier of the pulses [30]. The frequency offset can be expressed as :

$$f_0 = f_r \frac{\Delta\phi}{2\pi}. \tag{2.9}$$

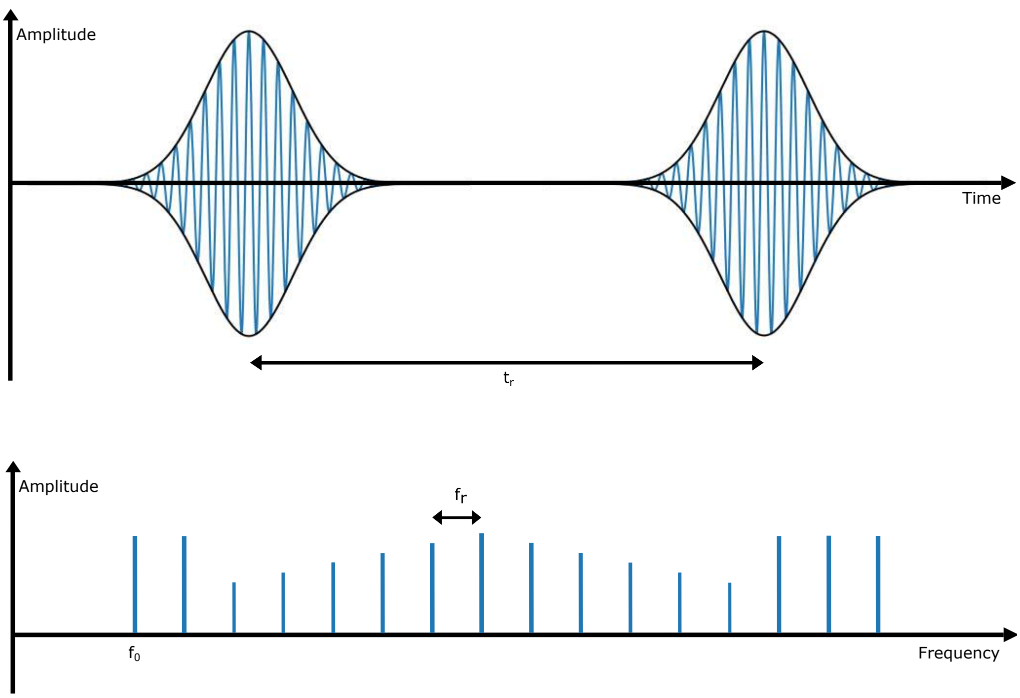

Figure 2.5: Time and frequency frame for a mode-locked pulsed laser, reproduced from [2].

To measure the ECDL linewidth, its beam is combined with the comb beam. This technique is called heterodyning. Let's consider two beams that are combined, using a beamsplitter for example, with their respective fields :

$$E_1(t) = E_{01}\, e^{i(\omega_1 t + \phi_1)} \text{ and } E_2(t) = E_{02}\, e^{i(\omega_2 t + \phi_2)} \tag{2.10}$$

with ω_i their respective angular frequencies and ϕ_i their phases. The beat signal, with a field $E(t) = E_1(t) + E_2(t)$, is detected by a photodiode and has an intensity given by :

$$I(t) = |E(t)|^2 \implies I_{detected}(t) = A + E_{01}E_{02}\cos((\omega_1 - \omega_2)t + (\phi_1 - \phi_2)), \tag{2.11}$$

where A is a constant representing the DC offset of the detected signal and where we only keep the $\omega_1 - \omega_2$ components because the $2\omega_1$, $2\omega_2$ and $\omega_1 + \omega_2$ are oscillating too fast to be detected by the photodiode [31]. The beat frequency spectrum is obtained by Fourier transform [32]:

$$S_b(\nu) = \frac{\Delta\nu}{2\pi}\left[(\nu - \nu_b)^2 + \left(\frac{\Delta\nu}{2}\right)^2\right], \tag{2.12}$$

with $\Delta\nu$ the linewidth of the beating signal and ν_b its frequency. If the linewidth of the reference laser is equal to the linewidth of the probed laser, $\Delta\nu$ is twice the probed laser linewidth. If the reference laser linewidth is much smaller than the probed laser's, the beat linewidth will then be approximately the probed laser linewidth.
This technique is used because we consider that the comb linewidth is smaller than the ECDL linewidth, and therefore the measured linewidth is approximated to be the laser linewidth.

The spectral profile of the ECDL is assumed to follow a Voigt distribution, the convolution of a Gaussian and a Lorentzian profile [33]. Mathematically, the Voigt profile $V(f)$ is expressed as :

$$V(f) = \int_{-\infty}^{+\infty} G(f')L(f - f')df', \tag{2.13}$$

where $G(f)$ is the normalised Gaussian function and $L(f - f')$ is the normalised Lorentzian function. The overall full width at half-maximum (FWHM) of a Voigt profile, Δf_V, is estimated to be a combination of the Lorentzian and the Gaussian FWHMs [34]:

$$\Delta f_V \simeq a f_L + \sqrt{b f_L^2 + c f_G^2} \tag{2.14}$$

This approximation of the Voigt FWHM is used throughout this work to characterise the ECDL linewidth. The linewidth was calculated using the lmfit python library. The coefficients a, b and c used by the lmfit library are fixed as follows : $a = 1.0692$, $b = 0.8664$, and $c = 5.54083$.

The physical meaning behind this Voigt profile can be explained by the type of frequency noises present in lasers. The Gaussian part of the lineshape rises from the flicker noise which has a 1/f profile [35,36]. The Lorentzian part rises from the white frequency noise of the laser, which is inversely proportional to its output power. This Lorentzian lineshape originates from the spontaneous emission process [36, 37].

Another way to compute the laser linewidth is to use the power spectral density (PSD). The PSD frequency noise spectrum, $S_{\delta\nu}(f)$, is the Fourier transform of the autocorrelation function of the laser field. $S_{\delta\nu}(f)$ is expressed in $\mathrm{Hz}^2/\mathrm{Hz}$, and can be separated in two regions. The first one is at low frequency where the noise contributes to the linewidth, giving rise to the Gaussian lineshape. The other region is at higher frequencies, whose noise contributes to the wings of the lineshape, therefore not affecting the linewidth. These two regions can be separated by a line called the β-separation line. This behaviour is represented in Figure 2.6, and the FWHM of the laser linewidth is computed with the formula [38]:

$$FWHM = \sqrt{8\ln(2)A}, \tag{2.15}$$

where A is the surface below the curve of the high modulation index area for the part of the $S_{\delta\nu}$ curve that is above the β-separation line.

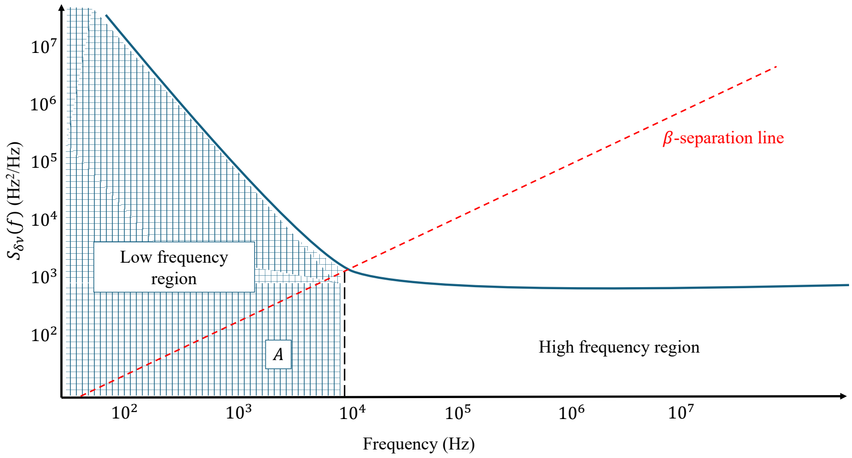

Figure 2.6: Illustration of the spectral density of the frequency noise of a laser, composed of flicker noise at low frequencies and white noise at higher frequencies, adapted from [38]. The red dotted line represents the β-separation line, with its expression given by : $S_{\delta\nu}(f) = 8\ln(2)f/\pi^2$. The area A used for the linewidth calculation is the area with the grid.

2.3.2 Allan deviation

The Allan variance $\sigma^2(\tau)$ is a statistical measure used to characterise the frequency stability of oscillators over different averaging time τ [2, 39]. Considering M samples $\bar{y}_k$ where each $\bar{y}_k$ represents the average of the quantity $y(t)$ over the time interval τ, the Allan variance is defined as :

$$\sigma^2(\tau) = \frac{1}{2(M-1)} \sum_{k=1}^{M-1} (\bar{y}_{k+1} - \bar{y}_k)^2 \equiv \langle(\bar{y}_{k+1} - \bar{y}_k)^2\rangle. \tag{2.16}$$

with $\bar{y}_k = \frac{1}{\tau}\int_{t_k}^{t_k+\tau} y(t)dt$, the averaging of $y(t)$.
Unlike classical statistical variance, Allan variance is based on the difference between adjacent frequency values and not on the difference between one frequency

value and the mean value.

The overlapping Allan variance is a refined Allan variance. It uses overlapping pairs of adjacent time intervals τ instead of being restricted by non-overlapping intervals, as used for the classical Allan variance. This development of the Allan variance improves its statistical efficiency because it uses the complete time dataset for each τ value [40]. Its analytical expression is given by :

$$\sigma^2_{overlap}(\tau) = \frac{1}{2(m\tau_0)^2(N-2m)} \sum_{n=1}^{N-2m} (x_{n+2m} - 2x_{n+m} + x_n)^2, \tag{2.17}$$

with $m\tau_0$ the considered averaging time, N the total number of samples and x_n the phase data of the time-series.
Practically, to compute the overlapping Allan variance of an oscillator, one performs measurements of the time signal of the oscillator, over the longest time interval possible, then computes the overlapping variance over the entire dataset.

The Allan deviation is the square root of the Allan variance. It is commonly represented on a log-log plot as a function of the averaging time τ. The different types of frequency noises introduced in the beginning of this section exhibit a characteristic behaviour in an Allan deviation plot, allowing a quick identification of the dominant noise sources in a system.
The flicker noise is independent of the averaging time, it follows a τ^0 law, therefore appearing as a flat region in the plot. The white noise is inversely proportional to the averaging time, depicting a τ^{-1} trend. On the contrary, random walk noise increases with the averaging time, following a τ^{+1} dependence [29]. By examining the Allan deviation curve, one can rapidly assimilate which type of frequency noise is affecting the system stability, as illustrated in Figure 2.7. The Allan deviation reaches a minimum at a certain averaging time τ when the system has reached its best stability.

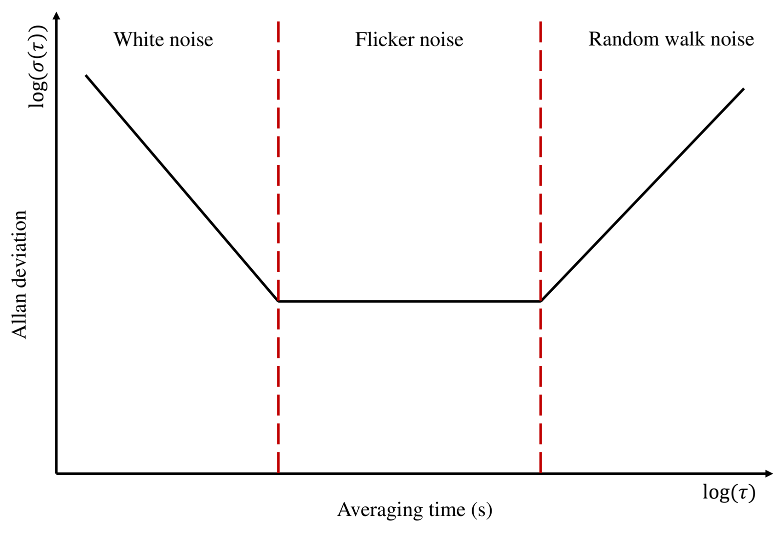

Figure 2.7: Illustration of the different frequency noise behaviours in an Allan deviation plot, inspired from [2].

3 Experimental setups

3.1 Presentation and assembling of the 1550 nm ECDL

As explained in Chapter 2, an External Cavity Diode Laser (ECDL) is composed of a laser diode, a lens, a grating, an output mirror and a piezoelectric transducer. The ECDL assembled for this master's thesis is based on the design by Dr. Alexandr Bogomolov and its schematic is shown in Figure 3.1. The laser diode (LD-1600-0050-AR-1 from Toptica Photonics) used in this setup has an anti-reflective (AR) coating. Therefore, it is not necessary to counteract mode competition as described previously. Moreover, this laser diode can be tuned from 1500 to 1630 nm but was used with a centre frequency of around 1550 nm during this work.

The first step was to align and focus the laser diode using a lens to position the focal point on the grating. The diode and lens are placed inside a tube, and focusing is achieved by precisely adjusting the position of the lens within this tube. Next, the grating was positioned such that its first-order reflection is directed back towards the laser diode. Fine alignment of the external cavity was performed using a flexion mount. This mount is connected to the plate holding the grating and the mirror. Modifying its vertical angle correspondingly adjusts the vertical angle of the grating. The next step involved optimising the angle of the laser diode's polarisation, as it is not specified by the laser diode datasheet. Adjusting the polarisation angle ensures that the incident light on the grating matches the polarisation for which the grating operates most efficiently.

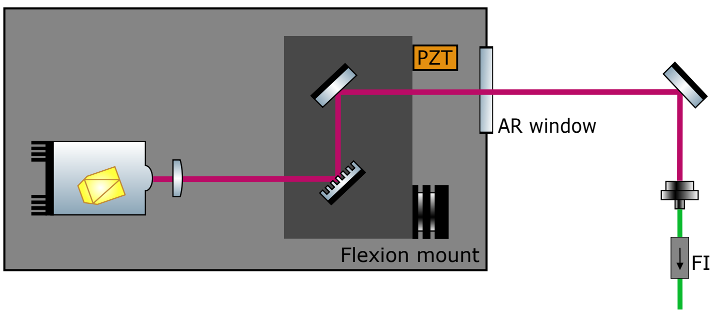

Figure 3.1: External Cavity Diode Laser schematics. PZT stands for piezoelectric transducer, FI stands for fibre isolator and AR stands for anti-reflective coating.

An anti-reflective coated window is placed as the output of the laser for thermal insulation. Due to the laser diode's sensitivity to thermal noise, the ECDL is temperature stabilised using a thermoelectric cooler (TECH3S from Thorlabs). The cooler is mounted underneath the ECDL box, in direct contact with the optical breadboard. One thermistor is placed beneath the laser diode, and another is placed below the ECDL box. The thermistors and the thermoelectric cooler are connected to a TEC controller (TEC1091 from Meerstetter engineering). This controller is set to a temperature of 22.05°C and is continuously powered to ensure temperature stabilisation of the ECDL. The AR-coated window minimise optical losses and serves to seal the enclosure, providing thermal insulation and isolating the ECDL from environmental temperature fluctuations.

3.2 ECDL beating with the frequency comb

To measure the linewidth of the ECDL, the beam is sent to a beating unit (DFC BCF and DFC MD from Toptica Photonics) with the frequency comb. The comb used for this work is the DFC system from Toptica that has a repetition frequency of 200 MHz and a linewidth of a few tens of kilohertz. This frequency comb, locked to a quartz GPS disciplined oscillator, has a stability of $2 \cdot 10^{-12}$ in 1 second [41]. The beating unit consists of a fibre combiner, a grating, and a photodiode.
The fibre combiner mixes the two beams from the ECDL and the comb, while simultaneously directing 1% of the ECDL beam to a wavemetre (WS7 Super Precision Wavelength Meter from HighFinesse Laser and Electronics System), allowing precise measurement of its frequency, with an accuracy of 40 MHz. The grating spectrally filters the frequency range of interest around 193 THz, corresponding to the ECDL output frequency. The resulting beat signal is detected by a photodiode and its output is sent to a spectrum analyser (SSA3021X from Siglent) to measure the beat note linewidth.
A spectrum analyser is an instrument used to measure the frequency spectrum and the power of a signal. The radio-frequency input signal is firstly filtered to ensure that it matches the passband of the instrument. This filtered signal is then mixed with a local oscillator to convert its frequency into an intermediate frequency that is suitable for analog-to-digital conversion (ADC). This ADC signal is the one that appears on the screen of the spectrum analyser [42].

3.3 Feedback loop of the PDH setup

The feedback loop consists of several electronical components. As explained in Section 2.2, the signal from the photodiode in reflection is mixed with the local oscillator signal. This mixed signal is then low-pass filtered before going into a PID controller. In this work, the low-pass filtered signal is sent into a lockbox.
This lockbox (FSC100 from MOGlabs) contains two controllers : a PID (proportional - Integral - Differential) controller and an integrator. The integrator acts on the slow output of the lockbox, which is connected to the piezoelectric transducer of the ECDL. This output compensates for the slow drift of the ECDL frequency. Meanwhile, the PID controller acts on the fast output, which is connected to the laser diode current. The lockbox generates a seesaw ramp with an amplitude of 1 V,

which is applied to both the PZT and the current of the ECDL to scan the cavity mode.

To achieve optimal locking, various parameters of the controller can be adjusted. A schematic representation of the frequency effect of these different parameters is shown in Figure 3.2. For the slow loop, the parameters are called the *slow integrator* and the *slow gain*. The slow integrator parameter adjusts the corner frequency of the servo integrator, from 25 Hz to 1 kHz (see arrow *b* in the figure). Additionally, this integrator can be switched from a single to a double integrator using one of the internal switches of the lockbox. The double integrator has a higher gain and a lower corner frequency, compared to the single integrator, ensuring a dominant response of the slow servo at low frequency. For the three locks described in the rest of this chapter, the slow integrator parameter was set to a double integrator.

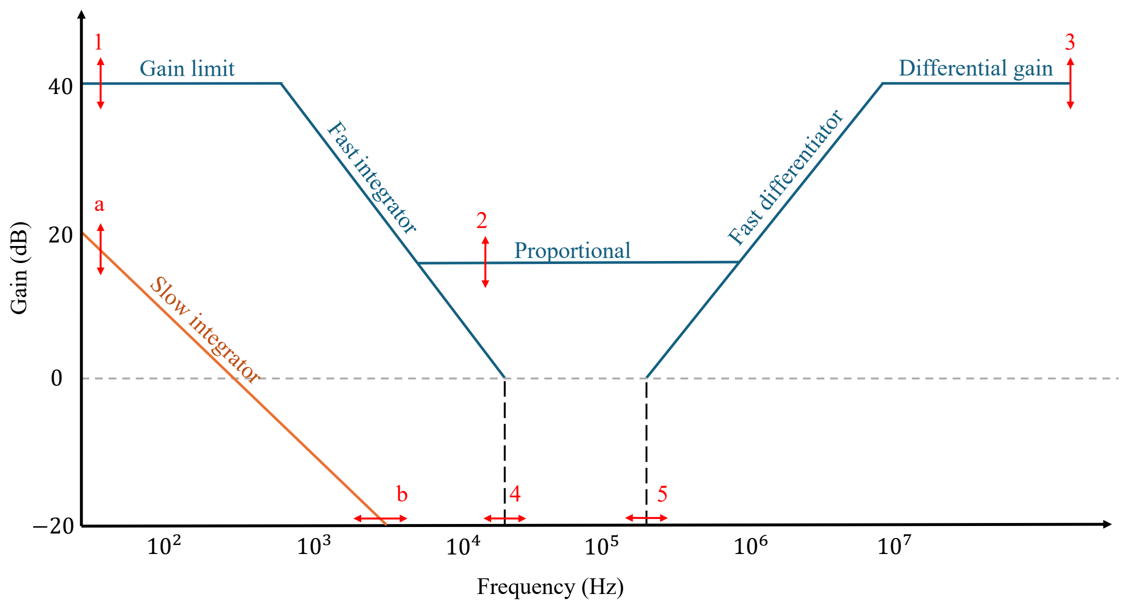

Figure 3.2: Schematic Bode plot of the lockbox action, adapted from [43]. In blue is the effect of the fast servo controller, and in orange, the slow servo controller.

In the fast loop, the PID parameters include the *fast integrator* and the f*ast differentiator*. These parameters adjust the corner frequency of the fast servo integrator and differentiator, respectively (see arrows 4 and 5 in the figure). The fast integrator corner frequency can range from 10 kHz to 2 MHz, while the fast differentiator corner frequency can be tuned from 100 kHz to 10 MHz. It is worth noting that the fast differentiator can be turned off, and a low-pass filter can be used instead. For this work, only the fast differentiator was used, without the low-pass filter. The *differential gain* parameter adjusts the gain limit at high frequencies, while the *gain limit* parameter adjusts the gain at lower frequencies (see arrows 3 and 1 in the figure).

Both the *slow gain* and *fast proportional gain* are adjusted using knobs without visual markers, and therefore, are not specified in the rest of this section. The slow gain can range from -20 dB to 20 dB, while the fast proportional gain can range from -10 dB to 50 dB (see arrows a and 2 in the figure).

The lockbox also has two switches associated to the fast and the slow feedback loops. These switches can be used to select the sign of these loops.

In the following sections, the different values of the lockbox parameters allowing a stable lock will be indicated.

3.4 PDH lock to a low-finesse cavity

After assembling the ECDL, the first test was to PDH lock it to a low-finesse cavity. The experimental setup for this test is shown in Figure 3.3.

In this setup, modulation is applied directly to the laser diode current at a frequency of 8 MHz, and amplitude of 20 mVpp. For this experiment, the local oscillator signal sent into the mixer had an amplitude of 1.4 Vpp. A phase shift of 90° is applied to the local oscillator to optimise the error signal. This phase shift is specific to the experimental setup, and will differ for each cavity lock. The mixer output is passed through a low-pass filter with a cutoff frequency of 5 MHz before entering the lockbox.

For this setup, the controller parameters allowing a stable lock were as follows:

- Slow integrator: 1 kHz
- Fast integrator: 20 kHz
- Fast differential: 2.5 MHz
- Fast differential gain: 6 dB
- Gain limit: 40 dB

The ECDL beam first passes through a half-wave plate to select its polarisation and to isolate the laser from the rest of the optical setup. The beam then passes through a polarising beamsplitter (PBS), which directs the reflected light from the cavity to the reflection photodiode. After the PBS, a quarter-wave plate changes the polarisation of the light, going from linear to circular, ensuring that the reflected light is directed back towards the PBS and into the photodiode. A lens, placed just before the cavity, ensures good mode-matching between the ECDL beam and the cavity. Mode-matching means that the waist of the laser beam coincides with the waist of the cavity, maximising the input beam injection into the fundamental transverse mode (TEM_{00}) of the cavity.

The cavity is 7.5 cm long and its input mirror has a reflectivity of 99.35%, while its output mirror a reflectivity of 99.9%, both having a radius of curvature of 100 mm. Therefore, the cavity has a finesse of approximately 800 ($\mathcal{F} = \pi\sqrt{R}/(1-R)$). This cavity characteristics correspond to a mode linewidth of 2.4 MHz and a free spectral range (FSR) of around 2 GHz.

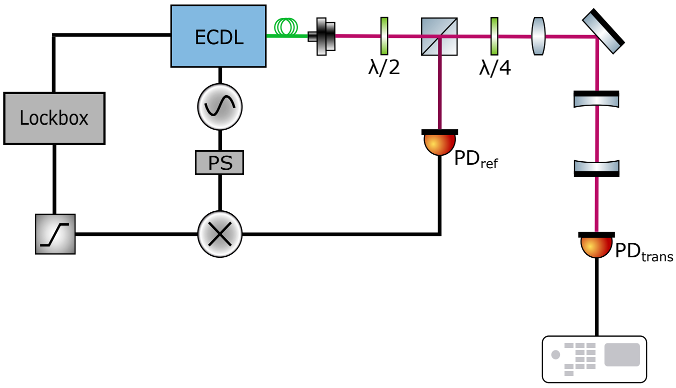

Figure 3.3: Experimental setup for PDH locking to a low finesse cavity. The electronical signal path is in black, the open air beam path is in red and the fibre beam path is in green. The half- and quarterwave plates are represented by the $\lambda/2$ and $\lambda/4$ components, respectively.

The first locks were achieved using this setup; however, the analysis of the locking stability, as presented in Section 4.2.1, was realised with the data taken from a same finesse cavity in the setup for the ULE cavity, as described in Section 3.6.

Locking the ECDL to a low-finesse cavity was the first step to understand and implement the PDH locking technique used in the rest of this work. This setup provided valuable insights into the operation of the lockbox and the tuning of its different parameters.

3.5 PDH lock to a high finesse cavity

The next step in implementing PDH locking was to lock the ECDL to a high-finesse cavity. The experimental setup for this experiment is shown in Figure 3.4.

The cavity used in this setup is part of the FANTASIO setup, which is used for Cavity Ring-Down Spectroscopy [44]. The finesse of this cavity can be calculated using the general definition of the finesse :

$$\mathcal{F} = \frac{\pi\sqrt{R}}{1-R}, \tag{3.1}$$

with R, the reflectivity of the mirrors. However, since the reflectivity of the cavity mirrors is not precisely known, this formula can be modified with the definition of the ring-down time τ [44]:

$$\tau = \frac{L}{c(1-R)}, \tag{3.2}$$

with L, the length of the cavity.
Then, by assuming that $R \to 1$ and therefore $\sqrt{R} \simeq 1$, the finesse can be expressed as :

$$\mathcal{F} \simeq \frac{\pi c \tau}{L}. \tag{3.3}$$

For this cavity, the ring-down time was measured to be $\tau = 180\,\mu$s, the length of the cavity is $L = 75$ cm, and the speed of light, $c = 3 \cdot 10^8$ m/s. Using these values, the finesse is calculated to be $\mathcal{F} \simeq 200\,000$. With a FSR of 200 MHz, the cavity mode linewidth is:

$$\Delta\nu = \frac{FSR}{\mathcal{F}} = 884 \text{ Hz}.$$

In this setup, the modulation of the laser field is performed using an EOM, driven by a 25 MHz local oscillator with an amplitude of 20 mVpp. The switch to using the EOM (NIR-MPX-LN0.1 from iXblue photonics) was necessary because the ECDL current driver has a bandwidth limit of 10 MHz, which is insufficient for such a high modulation frequency. The feedback loop correcting the ECDL output frequency includes the same mixer and lockbox used in the previous setup. A 25 MHz signal with an amplitude of 1.4 Vpp and a phase of 160° is sent into the mixer along the signal from the photodiode in reflection. The low-pass filter in this setup has a higher cutoff frequency, 32 MHz, than in the low-finesse setup to accommodate the higher modulation frequency. A Booster Optical Amplifier (BOA) (BOA1550S from Throlabs) is introduced to increase the ECDL output power, which is otherwise too low to observe a signal in transmission of the cavity. Since this experiment was implemented in an already existing experimental setup, the optical layout was constrained by pre-existing optical components. Consequently, the half-wave used in the previous configuration was replaced with a fibre polarisation controller (FPC), while the quarter-wave plate was still used.
The lockbox parameters used for this experiment are as follows:

- Slow integrator: 50 Hz
- Fast integrator: 100 kHz
- Fast differential: 1 MHz
- Fast Differential gain: 12 dB
- Gain limit: 30 dB

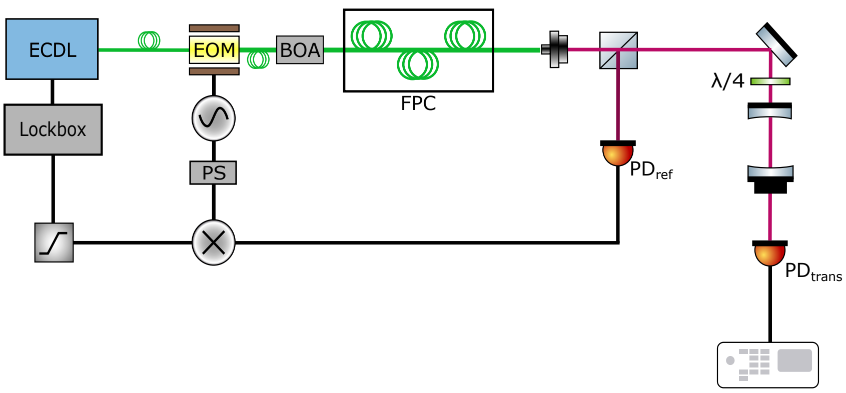

Figure 3.4: Experimental setup for PDH locking to a high-finesse cavity. The electronical signal path is in black, the free-space beam path in red and the in fibre beam path in green. BOA means Booster Optical Amplifier and FPC means fibre Polarisation Controller.

3.6 PDH lock to a mechanically stable etalon

The last experiment in this thesis was to lock the ECDL to a mechanically stable optical cavity. The etalon used for this experiment consists of two mirrors encased within an Ultra Low Expansion (ULE) cylinder. ULE glass is a material with a very low thermal expansion coefficient, $0 \pm 30 \cdot 10^{-9}$ / °C between 5°C and 35 °C [45], making it highly suitable for mechanically stable optical cavity implementation. The ULE cavity is placed inside a vacuum cavity, around which a thermal band is wrapped. This experiment was first carried out without pumping the cavity or temperature controlling it. Afterwards, the ECDL was locked to the cavity while it was temperature stabilised to 32°C. Then, it was re-locked when the cavity was under vacuum, down to $1.5 \cdot 10^{-4}$ mbar, and temperature stabilised. This temperature is the temperature of the vacuum cavity and not the actual ULE cavity because the thermal sensor is placed on the external wall of the vacuum cavity. Similarly, the pressure value is read on a gauge placed before the cavity. The tube connecting the pump to the cavity, after the gauge, has a small diameter, so this pressure value is actually smaller than the actual pressure inside the cavity. This cavity is mounted vertically on the setup because this orientation is more mechanically stable.

The mirrors of this cavity have a reflectivity of 99.975% for the input mirror and 99.97% for the output mirror, with a radius of curvature of 1 m and 500 mm, respectively. The finesse of this cavity is $\mathcal{F} \simeq 11000$, its FSR is 2 GHz and its mode linewidth is 175 kHz.
As can be seen in Figure 3.5, the feedback loop of this setup is identical to the one used in the previous experimental setups. The modulation signal sent to the mixer has a frequency of 25 MHz, an amplitude of 1.4 Vpp and a phase of 80°, while the one sent to the EOM has a frequency of 25 MHz and an amplitude of 20 mVpp.

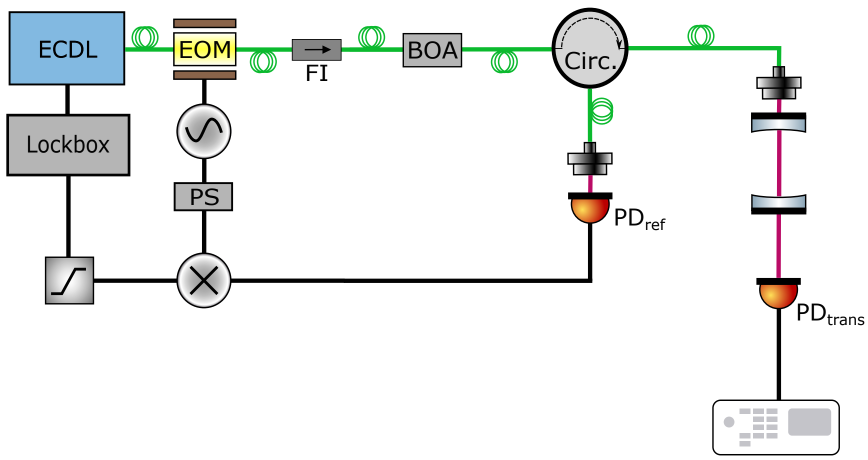

Figure 3.5: Schematics of the experimental setup used to lock on the stable etalon. Circ. is a fibre circulator, it replaces the polarised beamsplitter and the waveplates from the open air setup.

In this setup, the optical path was switched from an open-air path to a fully fibre-coupled path due to the cavity configuration. A fibre circulator replaces both the wave plates and the polarising beamsplitter. This circulator has three ports: one

port receives the ECDL beam, another sends the light to the cavity and the third port directs the reflection from the cavity to the reflection photodiode. After the EOM, another circulator is used as a fibre isolator to prevent unwanted feedback when the cavity modes are scanned. The BOA from the previous setup is also used here to amplify the ECDL output power because the intensity of the laser is too low. The first lock, without temperature control or vacuum, was achieved with an open-air optical path between the circulator and the photodiode in reflection.
For this first, the lockbox parameters are as follows:

- Slow integrator: 100 Hz
- Fast integrator: 10 kHz
- Fast differential: 1 MHz
- Fast Differential gain: 18 dB
- Gain limit: 50 dB

For the second and third experiments, with the cavity under vacuum and temperature control, a new circulator, working at a centre frequency of 1550 nm, is used. Additionally, the photodiode in reflection is fibre-coupled, which reduces losses in the optical path. The reflection photodiode for this experiment (PDA10CS2 from Thorlabs) is different from the one used before (PD100-SWIR1 from Qubig) because the latter lacked a fibre coupling component. Due to this change in photodiode, the modulation frequency was reduced to 10 MHz, because of the smaller photodiode bandwidth of 13 MHz. The local oscillator signal sent into the mixer has a frequency of 10 MHz, an amplitude of 1.4 Vpp and a phase of 180°, while the one sent to modulate the beam had an amplitude of 20 mVpp. Because of this phase value, the lockbox signs switches can be used to select the sign of the feedback loop. There is therefore no need to play with the phase of the local oscillator.
For the lock while the cavity was under vacuum and temperature controlled, the lockbox parameters have been changed to:

- Slow integrator: 25 Hz
- Fast integrator: 200 kHz
- Fast differential: 1 MHz
- Fast Differential gain: 18 dB
- Gain limit: 60 dB

4 Results

4.1 Characterisation of the ECDL

The first thing that was measured for the ECDL was its tuning range. The laser diode datasheet tells us that the maximum tuning range of the diode is from 1510 to 1630 nm. By moving the PZT with the screw attached to it, the maximum tuning range obtained was of around 70 nm. This was the mechanical tuning but when the ECDL is used in experimental setups, the laser frequency needs to be tuned more precisely using a waveform generator. To do so, the PZT voltage of the ECDL was scanned with a ramp of increasing amplitude, from 4 mVpp to 5.48 Vpp. With this ramp, the tuning range was of 15 GHz.

The next thing to do was to measure its linewidth. Using the method explained in Section 3.2, the ECDL light was sent into a beating unit with our reference frequency comb. The linewidth of the comb is of a few tens of kHz. The beat note that would appear on the spectrum analyser has a certain linewidth which is the sum of the comb linewidth and the laser linewidth. Considering that the comb linewidth is much smaller than the ECDL linewidth, the linewidth was measured by acquiring the spectrum analyser data and fitting it with a Voigt profile. One of the many linewidth measurement is shown in Figure 4.1. Figure 4.2 displays the measured linewidth for each data acquisition, with the associated error from the fit. The average measured linewidth is 69 $\pm$ 54 kHz, as is represented with the black dotted line in this figure.

Something that needed to be considered for the ECDL is its sensitivity to environmental perturbations. The laser we built was, in the beginning, sensitive to acoustic and mechanical noise. This was observed during the first measurements, when people were talking in the room or when the door was opened then closed, which caused pressure change in the room. These changes in pressure affect the refractive index, which resulted in the beat note drifting on the spectrum analyser. Likewise, when the ECDL was used to scan a cavity's mode, we would see the transmission signal get more noisy as people talked around. This sensitivity was affecting the first measurements, broadening the beat note. The first measured linewidth was consequently of more than 300 kHz. To counteract this problem, the ECDL was placed in a homemade box, made of light-blocking plaques onto which foam was attached. This box has decreased dramatically the acoustic sensitivity of the ECDL. However, the laser was also observed to be sensitive to mechanical noise. When something touched the table or the ECDL in itself, the beat note would drift. This sensitivity also accounts for mechanical vibrations in the ground caused by the pumps operat-

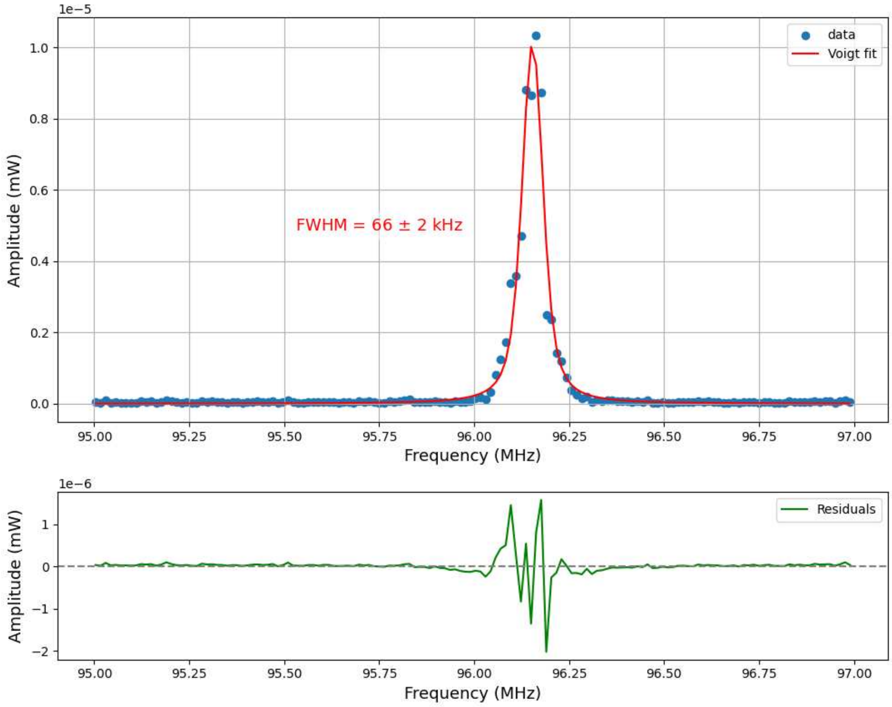

Figure 4.1: Example of a Voigt fit, in red, for one beat note measurement of the free running ECDL. The measured linewidth for this measurement was of 66 ± 2 kHz. The residuals of this fit are represented in green below.

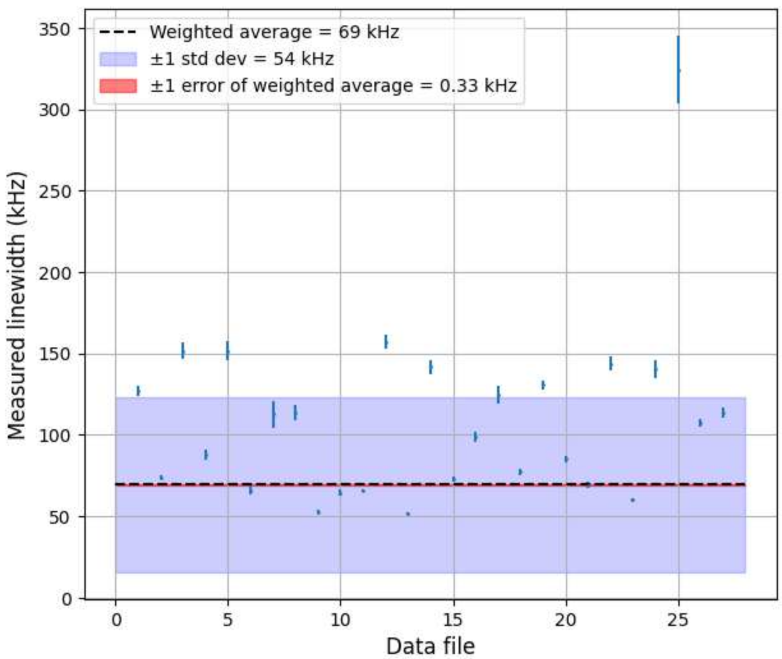

Figure 4.2: Linewidth measurements for every data acquisition for the free-running ECDL. The weighted average of these measurements is represented by the black dotted line, the error on the averaging is represented by the red box, and the standard deviation of this average is the blue box.

ing for other setups in the lab. This was resolved by placing the breadboard of the ECDL on three rubber holder pieces. This mechanical isolation also reduced the noise in the measurements.

Frequency stability

As explained in Section 2.3.2, the Allan deviation is a tool commonly used to illustrate the different noises affecting the system. To compute this deviation, a time trace of the beating is taken on an oscilloscope, with the highest time window possible. The instantaneous frequency is then extracted from this signal and is used to calculate the overlapping Allan variance using Equation 2.17. To obtain a physically meaningful result, the fractional frequency is used in this calculation. The fractional frequency is determined using the ECDL initial frequency measured on the wavemetre, 193.23466 THz. A more detailed explanation of the method used for Allan deviation calculation is presented in Appendix A.1.
Figure 4.3 shows this Allan deviation in blue. The behaviour of the Allan deviation curve corresponds to white frequency noise in the ECDL at really short averaging times. There is a small dip around $\tau \simeq 10^{-7}$ s, which may indicate a temporary region of stability. For longer averaging times, the decreasing trend indicates that the ECDL can reach a better frequency stability. However, this is the longest averaging time window that can be observed with the available instruments in the lab.

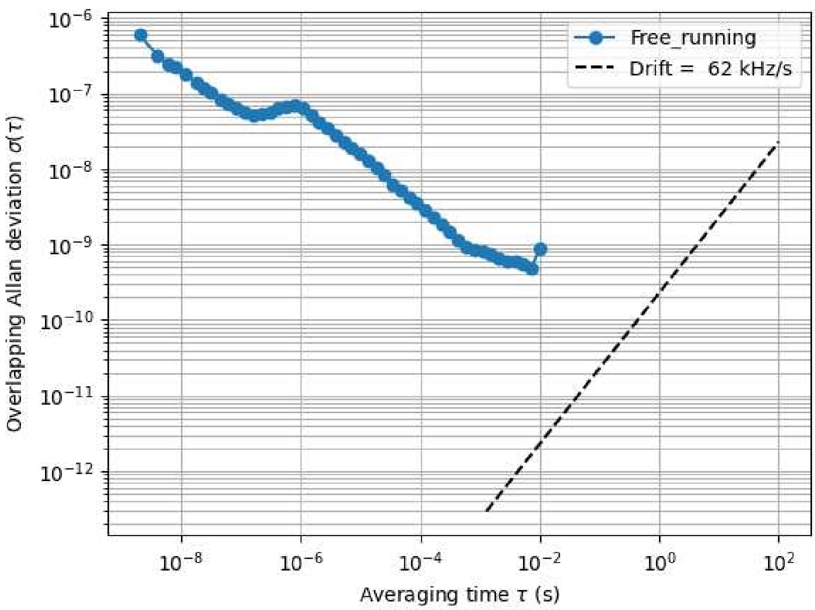

Figure 4.3: Allan deviation of the free-running ECDL. The black dotted line represents the drift trend.

During the measurement of the beat note, it was observed that its frequency would drift of 1 MHz in 16 seconds, which corresponds to a drift rate of 62.5 kHz/s. The black dotted line in Figure 2.16 represents the simulated behaviour of this drift rate, independently of the measured Allan deviation. The variance of this drift has a linear behaviour with the averaging time [46] :

$$\sigma_{drift}(\tau) = \frac{D\tau}{\sqrt{2}f_0}, \tag{4.1}$$

where D is the drift rate, in Hz/s, and f_0 is the ECDL frequency used to normalise the variance. This line was simulated to illustrate the expected drift behaviour at longer averaging times, which cannot be measured because of the limited maximum acquisition time of the oscilloscope. The measured Allan deviation curve stops before 10 ms because of this limited acquisition time. At some time τ, the system will reach its best stability point, and will afterwards be affected by Brownian noise, represented by the simulated drift. Due to limited resources, it was not possible to actually observe this best stability point.

4.2 Locking to the different cavities

4.2.1 Low finesse cavity

The results presented in this section were taken on the setup described in Section 3.4.

Locking stability

The observed signal in transmission of the cavity, representing the TEM_{00} of this cavity, and its associated error signal is represented in Figures 4.4a and 4.4c. The shape of the cavity mode does not match a Lorentzian lineshape, probably because of feedback into the ECDL.

Once the laser was locked to the cavity, the signal looked like the one shown in Figures 4.4b and 4.4d.
The signals in Figures 4.4a and 4.4b were taken on an oscilloscope that did not allow data acquisition. Therefore, the measurements to compute the stability of the lock were taken another day on another setup with the same finesse cavity. The stability of the lock looks different between the two setups because the mode-matching for the second setup was more difficult to achieve due to the vertical placement of the cavity. This placement limited the space between the fibre output and the input mirror of the cavity, therefore limiting the choice of lenses for good mode-matching.

The stability of the lock can therefore be computed from the trace in Figure 4.4d. To do so, the average standard deviation of the transmission signal is computed for all easurements. This standard deviation of the transmission signal was calculated to be 10 mV with an average intensity of 133 mV, as represented by the green line in Figure 4.4d. However, expressing this deviation in terms of an intensity does not mean much physically. This intensity variation can be translated to a frequency variation by a simulation of the cavity mode, with an amplitude of 141 mV, as shown in Figure 4.5. As can be seen in this figure, the standard deviation in intensity is used to find the variation in frequency. The translation works as follows: the minimum standard deviation intersects the cavity mode at two different points, represented by the blue dots on the figure. The frequency variation associated to the standard

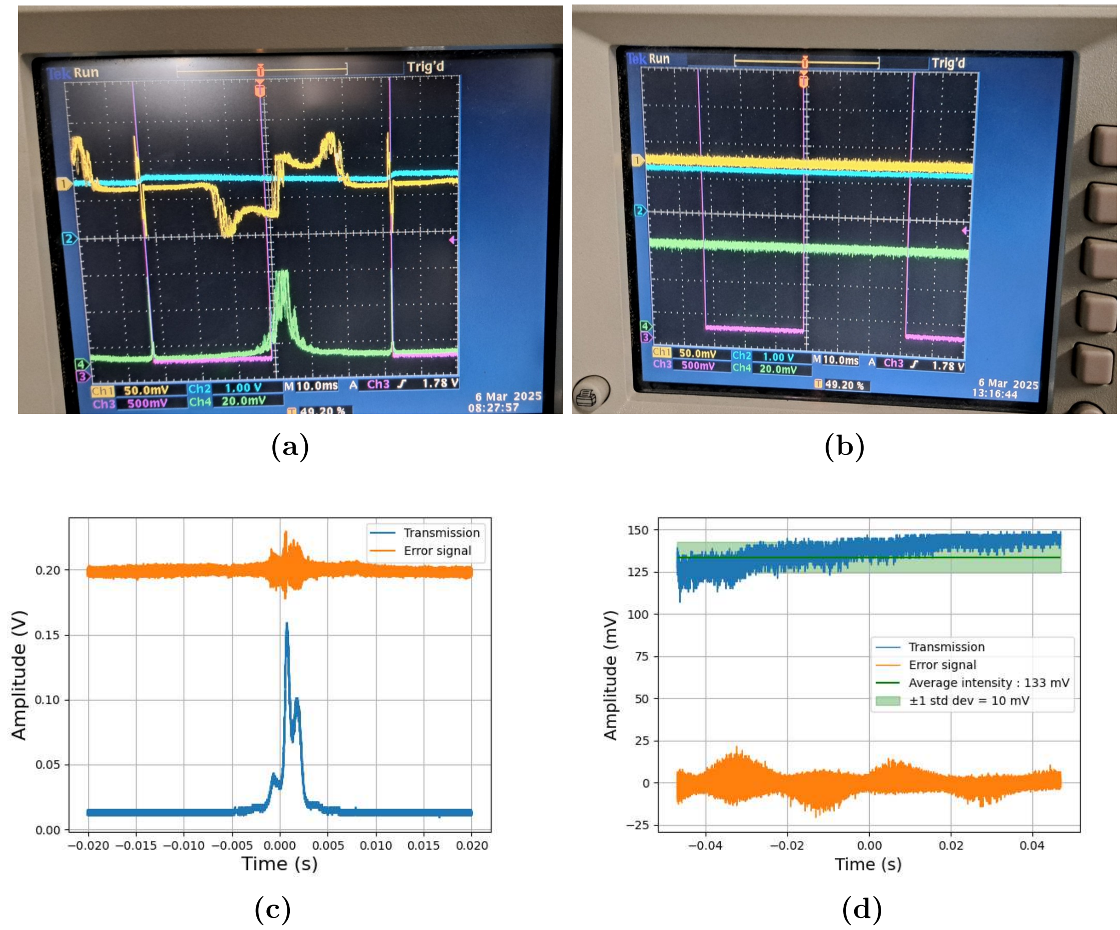

Figure 4.4: Traces of the cavity mode and its error signal and the corresponding locked signal. The pictures in (a) and (b) were with the lock achieved on the setup in open air. The plots in (c) and (d) were taken on the fibred stable etalon setup. The error signals in (a) and (c) have an offset to better distinguish them from the transmission signals. The green line in (d) represents the average measured intensity of the transmission, 133 mv, and the green box is the averaged measured standard deviation of this transmission signal when it was locked, 10 mV.

deviation of the intensity is the the frequency difference between these two points. This frequency variation is calculated to be of 935 kHz, which corresponds to around 39% of the cavity mode linewidth.

This result seems to be larger than what can be expected from a PDH lock. This large difference between the literature and the measurements is probably due to the signal-to-noise ratio (SNR) of the transmission signal. The noise in the locked transmission signal is probably due to a not sufficient mode-matching between the beam and the cavity. As explained in Section 3.4, the data taken for this analysis was taken on the ULE cavity setup. Therefore, because of the vertical configuration of this cavity, there was a spatial constraint that governed our choice of optical lens to focus the beam in the cavity. The locked signals in 4.4b seems to have a smaller standard deviation, a few mV, than the one presented in Figure 4.4d because of this mode matching. For the first setup completely in open air, there was enough space on the table to properly adjust the focus of the beam to the cavity input mirror, allowing a good mode-matching. Moreover, a part of the optical beam path was still in open air, which caused losses. Lastly, if the PID parameters are not rightly chosen, the transmission signal will be affected, and its standard deviation will increase.

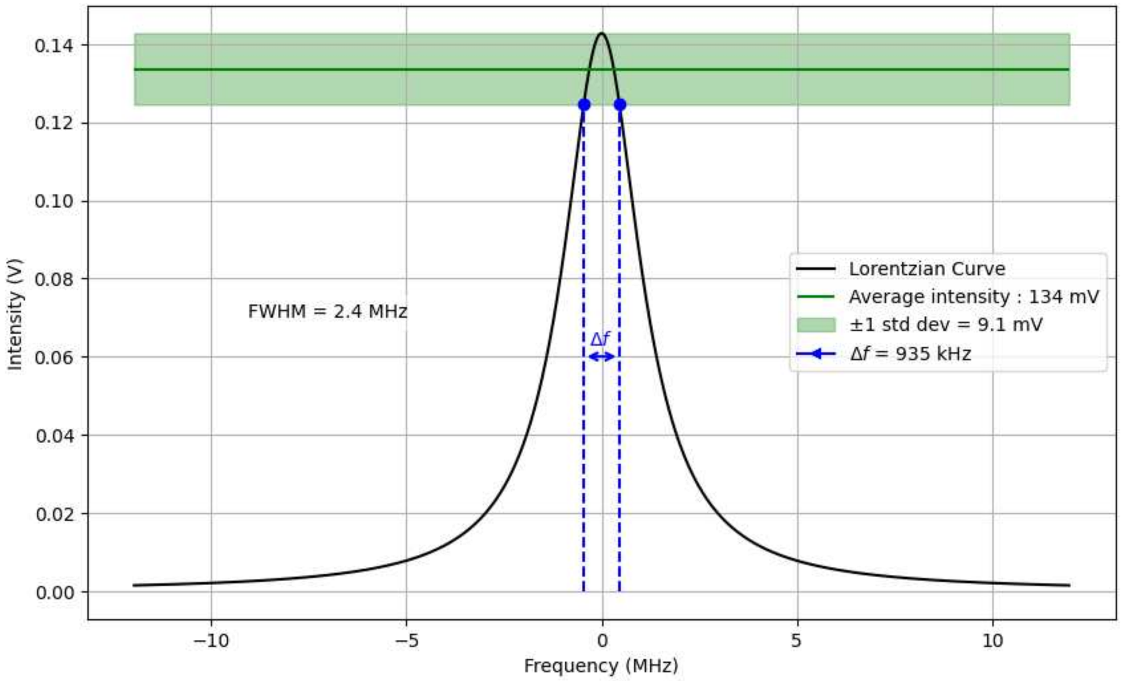

Figure 4.5: Simulation of the TEM_{00} cavity mode. In blue is the Lorentzian simulation, its amplitude is the averaged measured amplitude of this mode, 141 mV, and its FWHM corresponds to the theoretical FWHM of this cavity, 2.4 MHz. The green line represents the averaged locked intensity and the light green box represents the standard deviation of the locked transmission signals, averaged over all acquired data. The blue dotes represent the crossing between this standard deviation and the Lorentzian, allowing to translate a variation of intensity ΔI into a variation of frequency Δf.

Linewidth

Once the cavity was locked, measurement of the ECDL linewidth could be made using the technique described in Section 3.2.

A fibre splitter is placed right after the ECDL output and 10% of the beam is sent into the beat unit. The photodiode signal is read on the spectrum analyser and one of the beat note measurement is shown in Figure 4.6, along with its Voigt fit. The average of these measurements and their residuals is shown in Figure 4.6. On average, the measured line width was 151 kHz ± 61 kHz, as can be seen in Figure 4.7. This value is in the same range as the initial measurement of the ECDL linewidth. This is explained by the fact that the cavity modes are so large compared to the linewidth of the ECDL, 2.4 MHz compared to ± 100 kHz, that locking to the cavity only stabilises the beat note frequency drift and does not affect its width. This FWHM value is small compared to the frequency variation of the lock measured before because of the SNR as discussed before.

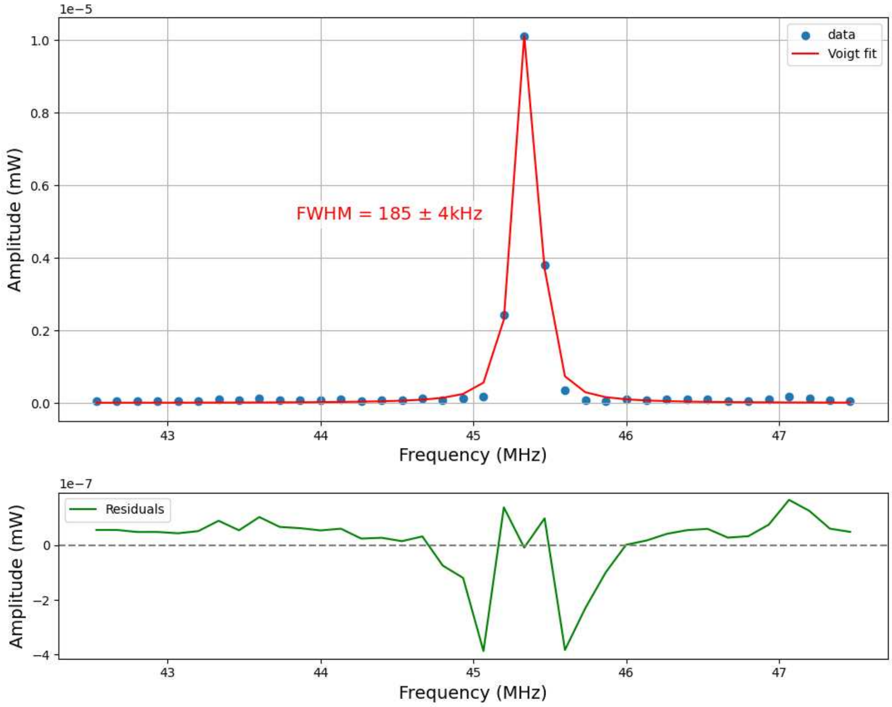

Figure 4.6: Example of one beat note measurement for the low finesse cavity. This beat note is fitted with a Voigt profile, in red, to measure its linewidth. The residuals from the fit are represented in green.

The linewidth can also be computed using the power spectral density of the transmission signal, as explained in Section 2.3.1. Practically, the locked transmission signal is firstly translated from intensity to frequency using the frequency variation computed above, 935 kHz. Afterwards, the signal is Fourier transformed, allowing to have the PSD of the locked ECDL, as shown in Figure 4.8. Then, the area under the curve for the part of the PSD that is above the β-separation line is computed, as represented in black in this figure. Using Equation 2.15, the linewidth is calculated to be of more than 4 MHz.

The computed linewidth is much larger than the one measured on the spectrum analyser because the signal used for this method is the transmission signal from the cavity. Therefore, this signal encompasses the laser noises but also the cavity noises. It also depends on how well the laser is locked to the cavity, i.e. the frequency stability of the lock. For this cavity, the stability of the lock is not that good, more than 30% of the cavity mode width. Another source of uncertainty in this method is the length of the time trace and its acquisition rate. Because this time trace is Fourier transformed, if there is not enough points in the time trace then the resolution of the FFT will be worse. The PSD will then be affected similarly, less points in the time trace will lead to a loss of resolution in the PSD. All of these influences, and the fact that the width of the cavity modes is of around 2 MHz, makes us think that the value obtained with the β-separation line gives an idea of the upper limit of the width of the cavity mode and not the actual linewidth of the ECDL.

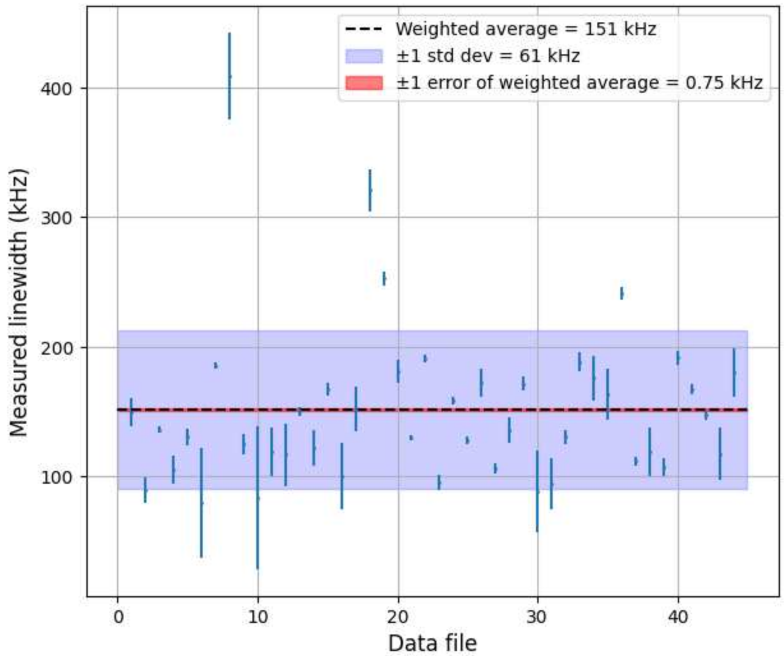

Figure 4.7: Measured linewidth per data acquisition for the low-finesse cavity. The weighted average of these measurements is represented by the black dotted line, the error on the averaging is represented by the red box, and the standard deviation of this average is the blue box.

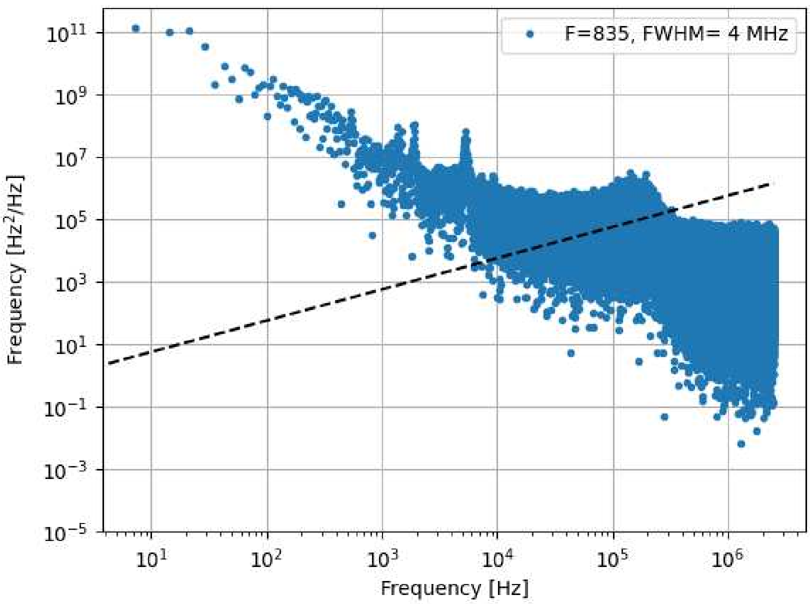

Figure 4.8: Power spectral density of the locked transmission signal for the low-finesse cavity. The β-separation line is represented in black on this plot.

4.2.2 High-finesse cavity

The next step was to lock on a high finesse cavity with the setup explained in section 3.5.

Locking stability

The cavity mode and its corresponding error signal can be seen in Figure 4.9a. The error signal does not have the typical shape of an error signal, as was simulated in Figure 2.4b, because of the really high-finesse, $\simeq$ 200 000 of the cavity and of the high modulation frequency, 25 MHz. Also because of the high-finesse of the cavity, of its length and therefore its decreased mechanical stability, the amplitude of the cavity mode was always changing. However, once the lock was achieved, the transmitted power into the cavity was quite stable and lasted for a few tens of minutes.

The locking stability of this lock is computed like before. First, the average of the standard deviation of the transmission signal is computed. This averaged standard deviation is of 14.2 mV, for an averaged intensity of 817 mV. Then, this intensity variation can be translated into a frequency variation by simulating a cavity mode, as shown in Figure 4.10. This simulated cavity mode has an amplitude of 831 mV, which is the averaged measured amplitude of the transmission, and its FWHM is the one computed in Section 3.5 : 884 Hz. This technique give us a frequency variation of 168 Hz, which corresponds to 19 % of the cavity mode linewidth.

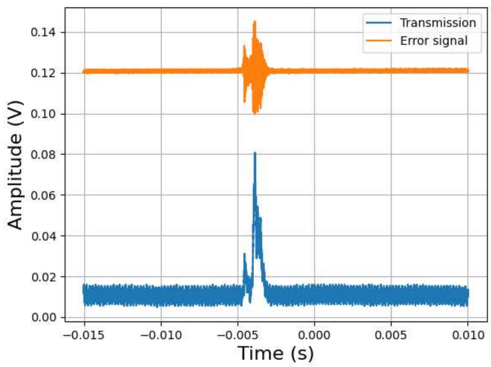

(a)

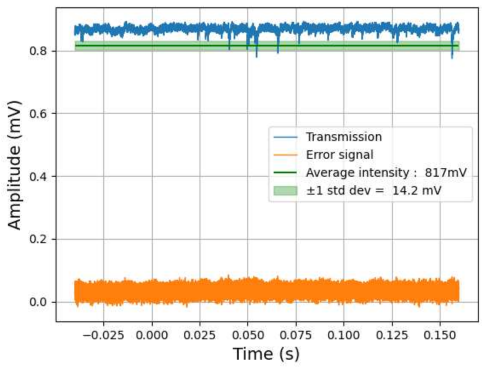

(b)

Figure 4.9: Examples of traces of the main cavity mode and the error signal in (a) and the locked signal in (b). The error signal in (a) has an offset of 0.12 V to better distinguish it from the transmission signal. The green line in (b) represent the averaged intensity of the locked signal, averaged over all the measurements, and the light green box is the standard deviation associated to these measurements.

This experiment showed that it was possible to lock our home-made laser to a fairly high finesse cavity with a relatively stable lock. This locking stability could be improved by using a completely fibred beam path instead of using a PBS. This fibre path would reduce the SNR in the locking signal, reduce the frequency variation of the lock, and most probably improve its stability.

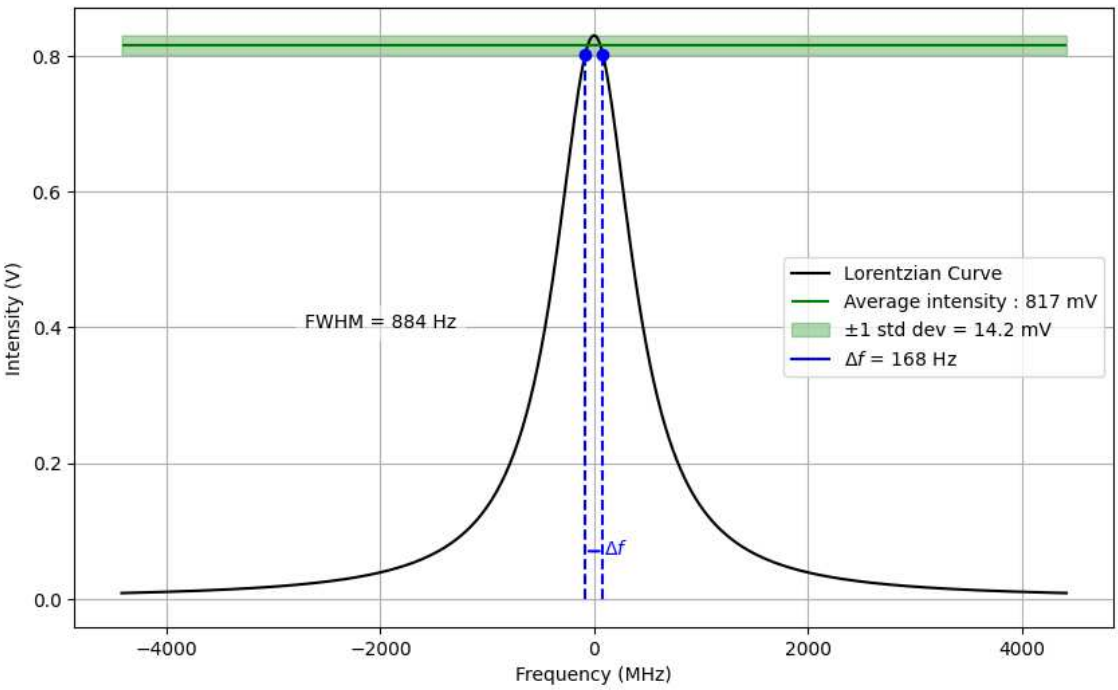

Figure 4.10: Simulation of the TEM_{00} mode of the high-finesse cavity with a Lorentzian profile. The green line is the average observed intensity of the locked transmission and the light green box represents the standard deviation of the locked transmission signal, averaged over all data. The blue dots represent where this deviation meets the Lorentzian, allowing to translate the variation of intensity ΔI into a variation of frequency Δf.

Linewidth

Once the cavity was locked, the linewidth of the beat note was measured. The procedure is the same as before, but this time, 90 % of the ECDL beam is sent to the beat unit with a fibre splitter, instead of 10%, like before because of the BOA used in the setup. The BOA amplifies the light enough so we do not need to send as much light towards the cavity.

The beat note data was taken from the spectrum analyser and Voigt fitted using the lmfit library. An example of one of the beat note measurement and its corresponding Voigt fit is shown in Figure 4.11. Figure 4.12 shows all the linewidth measurements with their associated errors. The averaged measured linewidth is then 30 ± 7 kHz.

When this value is compared to the locking stability of 168 Hz, there seems to be an incoherence between the two. The value of the linewidth is 3 order of magnitude higher than the variation in frequency. This can be explained by the frequency comb linewidth. In the beginning of this work, the linewidth of the frequency comb was assumed to be much smaller than the linewidth of the ECDL. But when the ECDL is locked to the high-finesse cavity, its linewidth is squeezed to follow the feedback loop of the locking process. Therefore, this linewidth becomes much smaller than the frequency comb linewidth and this measurement is most probably a measurement of the frequency comb linewidth instead of the ECDL's.

This theory can be confirmed using the β-line calculations. With the same pro-

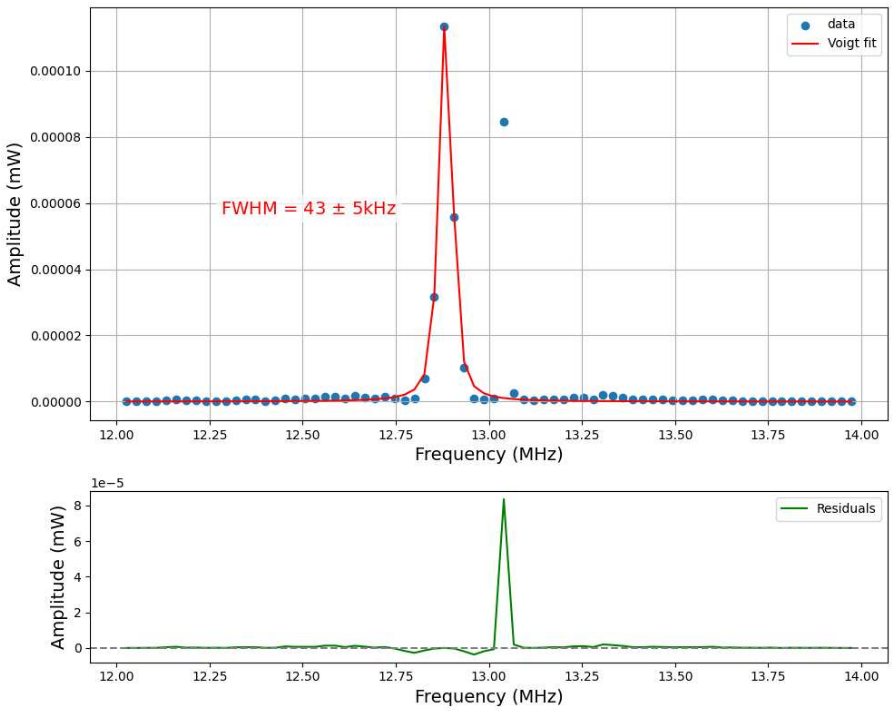

Figure 4.11: Example of one of the beat note measurements for the high-finesse cavity. For this measurement, the linewidth was computed from the Voigt fit, in red, and was computed to be of 43 ± 5 kHz. The residuals for the fit is also represented in green. The resolution on the spectrum analyser for this measurement was too low, which is why there is not many points defining the peak, leading to less accuracy in the fit.

cedure as before, we can use the power spectral density of the locked transmission signal to compute the linewidth of the ECDL. This method gives us a linewidth of 663 Hz, as illustrated by Figure 4.13, which corresponds to the measured frequency variation of the lock. Contrary to the low-finesse cavity measurements, this PSD calculation actually give us a more accurate upper limit to the real linewidth of the ECDL. With the beating measurement, we are limited by the comb's tooth linewidth. Therefore, if the linewidth of the ECDL is squeezed by the lock to the high-finesse cavity, making it much smaller than the comb linewidth, the beat note measurement cannot be trusted. The β-separation line method is then a great tool that gives an idea of the upper limit of the linewidth. The ECDL linewidth should be smaller than 663 Hz because this value is influenced by the cavity noise, the stability of the lock, the SNR of the transmission signal and the reliability of the Fourier transform. But because we do not have yet a narrow enough frequency reference, the PSD is the best tool to have an idea of this linewidth.

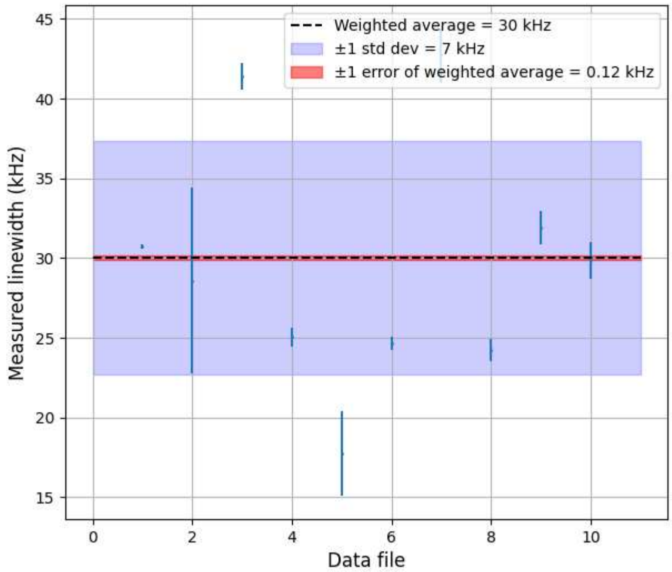

Figure 4.12: Measured linewidths for each data acquisition for the high-finesse cavity. The weighted average of all the measurements is represented by the black dotted line, the error on the averaging is represented by the red box, and the standard deviation of this average is the blue box.

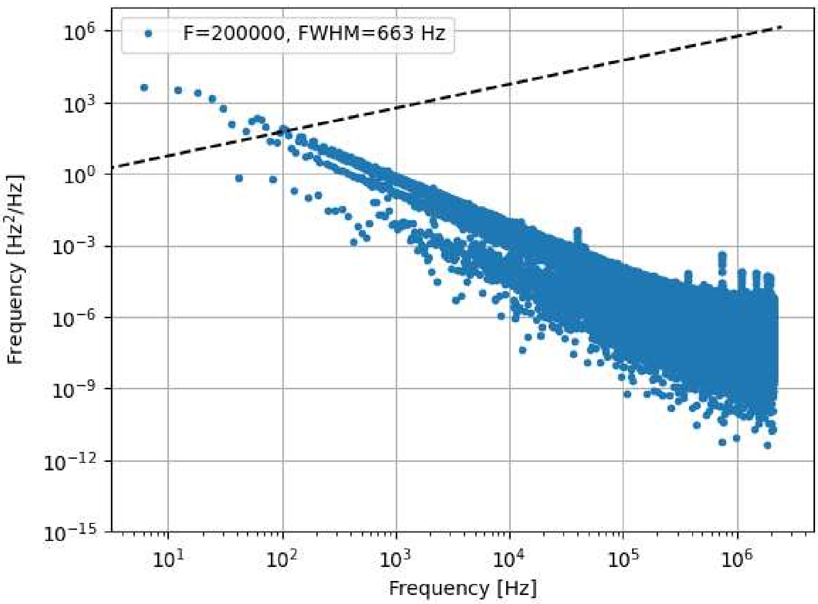

Figure 4.13: Power spectral density of the locked transmission signal for the high-finesse cavity. The black dotted line represents the β-separation line.

4.2.3 Mechanically stable cavity

This section presents the results obtained with the experimental setup described in Section 3.6.

Locking stability

The locking stability achieved for this cavity was done with three different conditions for the ULE cavity. The ECDL was locked to the ULE cavity when it was at ambient temperature an atmospheric pressure, then the ULE was temperature stabilised, and finally it was temperature stabilised and under vacuum. The observed cavity mode and error signal for the temperature controlled and under vacuum ULE are shown in Figure 4.14a. The SNR for these signal is better than the previous setup because of the completely fibred beam path. For this setup, the locking stability is computed using the locked error signal, as is shown in Figure 4.14c. Because the error signal for this lock is well defined, it can be used to express the deviation in intensity into a deviation in frequency. As it was explained in Section 2.2, the error signal is linear around resonance. It is then possible to compute the slope of this error signal around resonance, $\Delta I/\Delta f$, to find the relation between the standard deviation of the intensity and the variation in frequency. This slope is computed with a simulated error signal, as is shown in black in Figure 4.14c : $\Delta I/\Delta f = 0.2$ μV/Hz. Afterwards, the standard deviation of the locked error signal is calculated to be 3.31 mV, which leads to a frequency variation of 22 kHz or 12% of the cavity mode width, 175 kHz.

This frequency variation can be compared to the ones obtained with the same cavity but with different pressure and temperature conditions. For the ULE only temperature controlled, this deviation in frequency is computed to be of 26 kHz, which corresponds to 15 % of the mode width. For the ULE without any pressure or temperature control, the variation in frequency for the locked signal is computed to be of 56 kHz, which corresponds to 32% of the mode width.
As expected, with no stabilisation whatsoever of the cavity, the stability of the lock is a bit worse than with stabilisation because it is subject to random pressure and temperature fluctuations. The observed stability with temperature control only and temperature and pressure control are quite similar even if the temperature control only seems a bit more stable. This small difference is probably due to the pressure inside the cavity that had not reached its best stability level, whereas the temperature control has been on for a few days, reaching its stability.

Linewidth

After locking the ECDL to the cavity, the linewidth of the ECDL was measured. When the cavity was temperature controlled and under vacuum, the beat note looked like the one showed in Figure 4.15, and the averaged measured linewidth was of 27 $\pm$ 6 kHz, with a standard error of the weigthed mean of 0.16 kHz, as shown in Figure 4.16. The same measurements were done for the simple ULE and the temperature controlled ULE and the measured linewidths were 18 $\pm$ 6 kHz, with an error associated to the weighted average of 11 kHz, and 25 $\pm$ 7 kHz respectively, with an error associated to the weighted average of 0.16 kHz. It has to be noted that the value

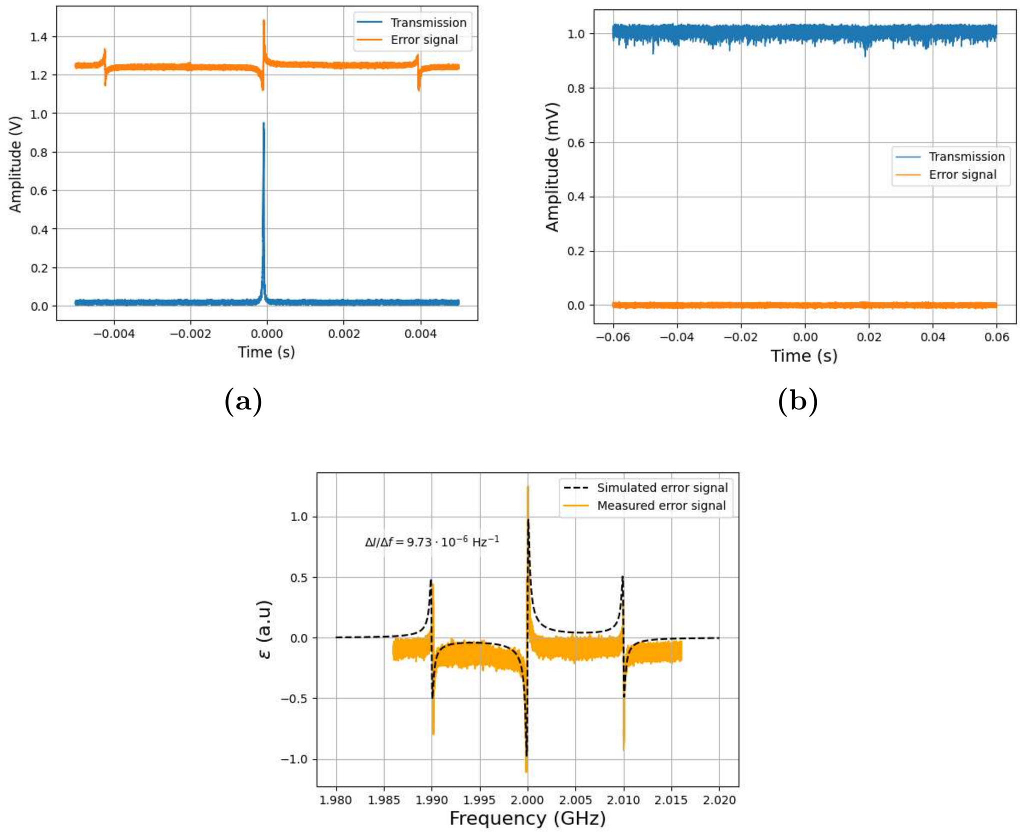

(a) **(b)**

(c)

Figure 4.14: Traces taken for the ULE under vacuum, $p = 2.5 \cdot 10^{-4}$ mbar, and temperature controlled, $T = 32$°C. Cavity mode and its corresponding error signal in (a). The displayed error signal has been artificially amplified in both amplitude, by a factor 10, and offset, by 1.3 V, to better distinguish its shape. Both locked signals, transmission and error signals, are displayed in parallel in (b). A close-up of the error signal is shown in (c) in orange, with the simulated error signal, in black. The measured signal has been normalised because the theoretical error signal is unitless. The simulated slope of the error signal around the resonance is $\Delta I/\Delta f = 0.2$ μV/Hz.

obtained for the ULE not under vacuum and not temperature controlled is smaller but with a higher error because of the resolution of the spectrum analyser used for the data acquisition. The resolution of the analyser was set to 10 kHz, which is too high for a measuremnt of the same magnitude. The measurements for the ULE temperature controlled and under vacuum were taken with a lower resolution and a smaller frequency interval, allowing to have more points defining the beat note, and therefore allowing a more precise fit.

These values for the linewidth of the ECDL are in the same magnitude, around 30 kHz, which could be once again the linewidth of the frequency comb and not the actual ECDL linewidth. We can compare these values to the ones obtained with the power spectral density of the locked transmission signal. The results of the computations for all three different conditions of the ULE are shown in Figure 4.17. As shown in this figure, the computed FWHM of the ECDL are 261 kHz for the not stabilised ULE, 102 kHz for the temperature controlled ULE and 125 kHz for the pressure and temperature controlled cavity. These values are one order of magnitude greater than the ones measured on the spectrum analyser, and in the same range as the cavity mode width of around 175 kHz.

Both methods give values that are close to the element of reference, the comb tooth linewidth and the cavity mode width. The β-separation line technique does not confirm if the linewidth is smaller than the comb tooth or not. If we look at the frequency variation of the lock, which was in the order of 30 kHz or more, then it would make sense that the linewidth would be a bit larger than this value. The linewidth could be in the 30 kHz to around 150 kHz range, but we do not have the tools yet to accurately measure it.

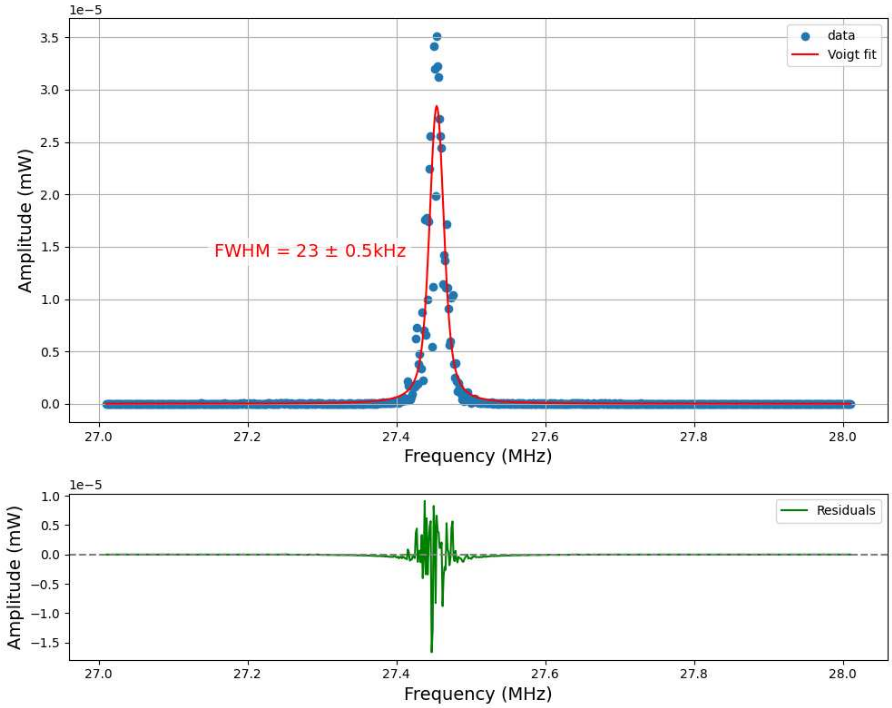

Figure 4.15: Example of one beat note measurement for the temperature controlled and under vacuum, $p = 2.5 \cdot 10^{-14}$ mbar, ULE cavity. The Voigt fit of this beat note is represented in red and from it, a FWHM of 23 ± 0.5 kHz was computed. The residuals of this fit is represented in green.

Frequency stability of the locked ECDL

Similarly to the free-running ECDL, the overlapping Allan deviation has been computed for the locked ECDL to the temperature and pressure controlled ULE cavity. The technique is the same as explained in Section 4.1, and the corresponding result is shown in Figure 4.18. This system's frequency is affected by white frequency noise at small averaging times. Contrarily to the free-running ECDL, there is no stability plateau around $\tau \simeq 10^{-7}$ s, which probably means that locking to the stabilised ULE cavity is actively suppressing frequency fluctuations at these lower timescales. The decreasing trend of the locked ECDL deviation shows that locking improves the frequency stability of the laser. Once again, there is a limitation due to the maximum acquisition time of the oscilloscope. It is therefore not possible to confirm how

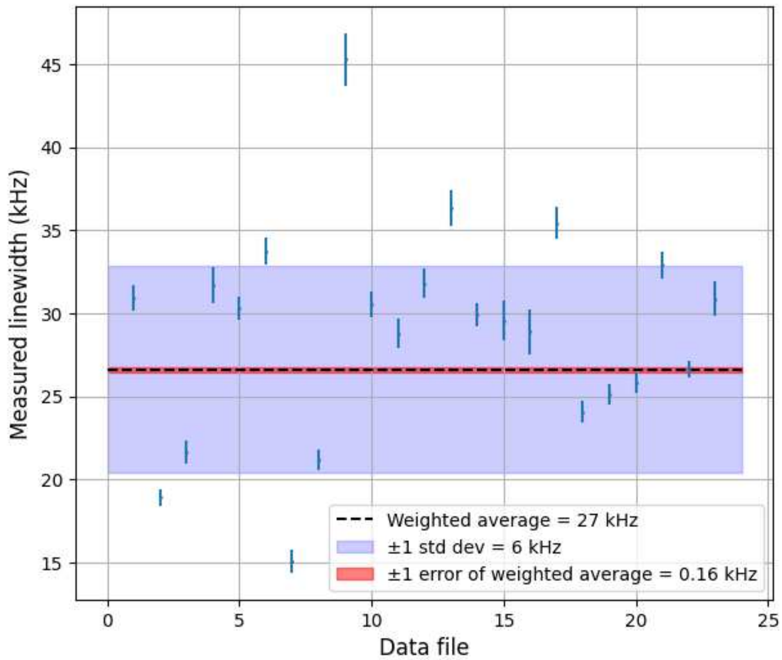

Figure 4.16: Mesured linewidth for different data acquisition. The weighted average of these measurements is represented by the black dotted line, the error on the averaging is represented by the red box, and the standard deviation of this average is the blue box.

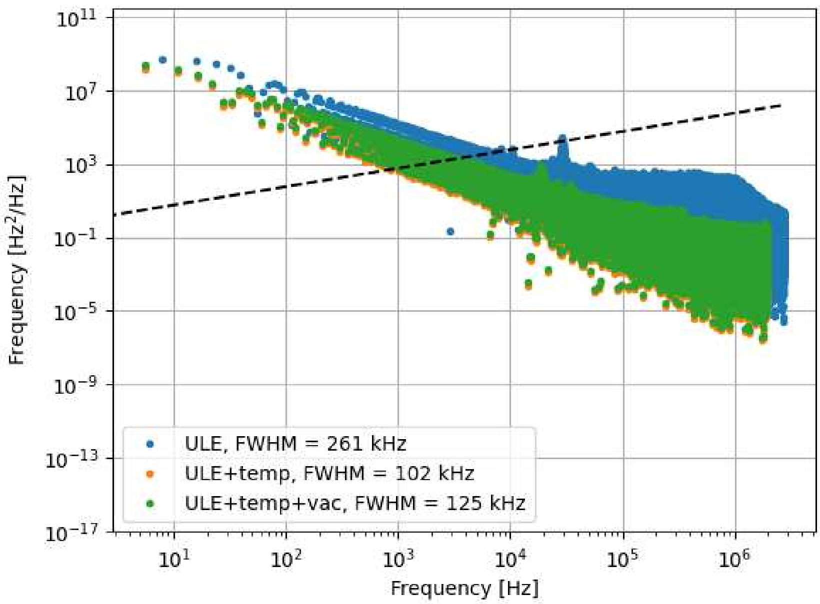

Figure 4.17: Power spectral densities of the locked transmission signal for the ULE cavity. The blue trace is for the transmission signal of the ULE whithout any temperature control or vacuum, the orange trace is for the ULE temperature controlled and the green trace is for the ULE temperature controlled, $T = 32°\text{C}$, and under vacuum, $p = 2.5 \cdot 10^{-4}$mbar. The black line represents the β-separation line.

well the feedback loop stabilises the ECDL frequency over longer averaging times. Using Equation 4.1, it possible to simulate the expected behaviour of the Allan deviation at longer averaging time, based on the measured drift rate of 30 kHz/s. The extrapolated drift line suggests that the system is likely to reach its stability limit at longer averaging time, beyond which it will be mostly influenced by Brownian noise.

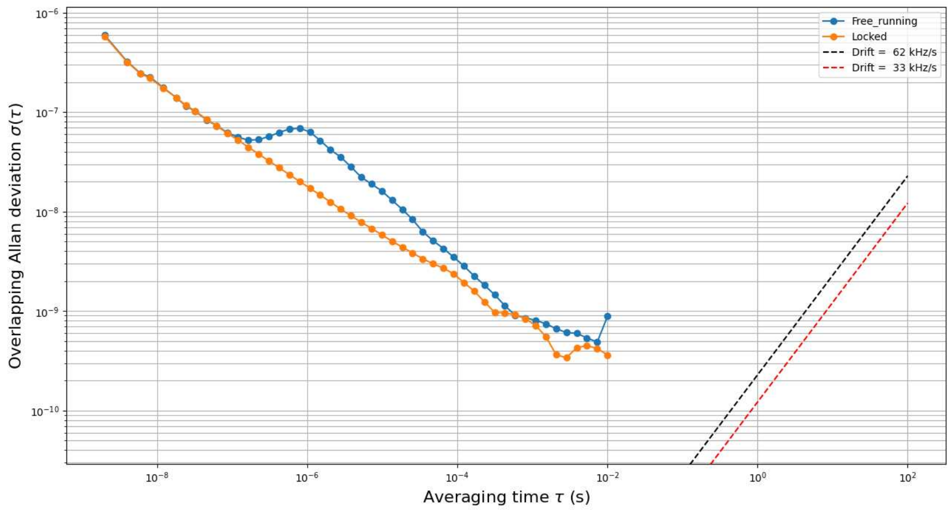

Figure 4.18: Allan deviation of the locked ECDL to the temperature controlled and under vacuum ULE cavity, in orange, compared to the deviation of the free running ECDL, in blue. For these measurements, the ULE cavity was at a temperature of 32.4°C and a pressure of $1.8 \cdot 10^{-4}$ mbar. The drifts of the free-running and locked ECDL are represented by the black dotted line and the red dotted line respectively.

Drift of the beat note

As explained before for the free-running ECDL, it was observed that the beat note was drifting over time. Once the ECDL was locked to the cavity, this drift has been observed to be reduced. Figure 4.20 shows the evolution of the beat note frequency when the ECDL was locked to the ULE cavity which was at room temperature and not pumped. Over the course of 2 hours, the beat note has drifted of around 15 MHz, which corresponds to a drift rate of 2 kHz/s. This drift is caused by the constant change in pressure and temperature of the cavity's environment. The influence of the pressure on the frequency drift can be observed with the measurements shown in Figure 4.20. For this measurement, the cavity was pumped down to around $7 \cdot 10^{-2}$ mbar then the pumps were switched off and the measurements were acquired after this switching off. There are two traces on this figure because the cavity unlocked at some point so it was re-pumped to the same level. For a total pressure variation of $\Delta p = 2.8 \cdot 10^{-1}$ mbar, the frequency has drifted of around $\Delta f = 130$ MHz. This gives a drift rate associated to the pressure of 1 Hz per $2.2 \cdot 10^{-9}$ mbar.

Then, the ULE cavity was moved to another room, and temperature stabilised to 32°C. The observed drift rate when the ECDL was locked to the cavity was of around

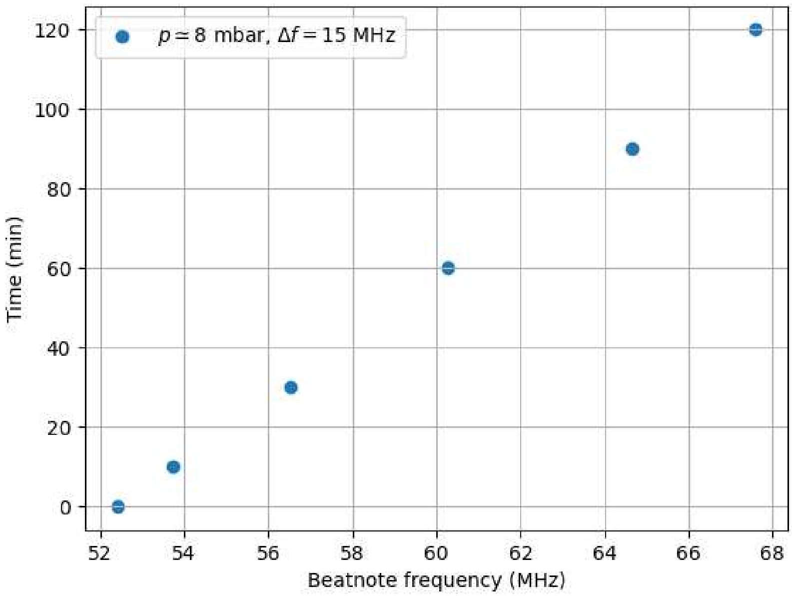

Figure 4.19: Evolution of the beat note frequency when the ULE cavity not temperature stabilised nor pressure controlled.

33 kHz/s. Afterwards, the cavity was put under vacuum and measurements of the beat note frequency were made during the pumping, as shown in Figure 4.21. these measurements showed that for a variation of pressure of $\Delta p = 2.4 \cdot 10^{-3}$ mbar, the frequency had drifted of $\Delta f = 19$ MHz, which corresponds to a drift of 1 Hz per $1.3 \cdot 10^{-10}$ mbar.

This drift is associated to the change in pressure which will affect the refractive index inside the cavity. If we consider that the refractive index of air at 1 bar is $n = 1.00027$ [47], the variation of frequency due to a variation of pressure can be computed using the free spectral range formula :

$$f = \frac{c}{2nL} \implies n = \frac{c}{2Lf} \tag{4.2}$$

where c is the speed of light, and L is the length of the cavity. A small variation of the refractive index Δn will therefore cause a small variation of the frequency Δf :

$$\frac{\Delta n}{\Delta f} = -\frac{c}{2Lf^2} = -\frac{n}{f} \implies \frac{\Delta n}{n} \simeq \frac{\Delta f}{f}. \tag{4.3}$$

Then, because the refractive index of air is considered to be 1 at 0 bar, the variation of the refractive index due to the variation of pressure at 1.5 µm is: $\Delta n = 2.7 \cdot 10^{-4}$ for a variation of pressure $\Delta p = 1$ bar. For the ECDL, which has a frequency of roughly 200 THz, the variation of frequency is of $\Delta n \cdot f = 5.4 \cdot 10^{10}$ Hz, for a variation of pressure of 1 bar. This rough calculation gives then a rate of 1 Hz per $2 \cdot 10^{-8}$ mbar.
This value is different than the one measured, and expressed before, probably because both pressure gauges for both measurements do not measure the actual pressure inside of the ULE cavity due to their placement. But, their measurements give

an idea of how the pressure evolved in the cavity. To avoid a drift due to pressure change, the ULE should then be brought to a pressure below 10^{-8} mbar.

The same reasoning can be done to associate a drift to a temperature variation affecting the ULE glass. Knowing that the thermal expansion coefficient of this material is $\alpha_{ULE} = 30 \cdot 10^{-9}$/K between 5°C (278.15 K) and 35°C (308.15 K), the variation in length due to a variation of temperature, assuming that it is indeed linear, is expressed as [48]:

$$\Delta L = \alpha L_0 \Delta T. \tag{4.4}$$

Taking Equation 4.2, we can express :

$$\frac{\Delta f}{\Delta L} = -\frac{c}{2L^2 n} \implies \frac{\Delta f}{f} \simeq \frac{\Delta L}{L} = \alpha \Delta T. \tag{4.5}$$

Once again, using the ECDL's frequency $f = 200 \cdot 10^{12}$ Hz, the frequency drift associated to a temperature variation of the cavity is $\Delta f / \Delta T = 6$ MHz/K, or similarly, 1 Hz per 167 nK. This thermal drift dominates if the cavity is pumped but if there is still air in the cavity, the temperature variation will affect mostly the refractive index in this cavity.

Considering that the refractive index of air at 15°C (288.15 K) is $n_{air} = 1.000272935$, and at 30°C (303.15 K) is $n_{air} = 1.000258934$ [49], this gives a variation of the refractive index of $\Delta n = 1.4 \cdot 10^{-5}$ for a temperature variation of $\Delta T = 15$ K. We can then find that for a temperature variation of 1°C, the variation of refractive index is of $\Delta n = 9.3 \cdot 10^{-7}$. Using Equation 4.3 and the laser initial frequency, 200 THz, the frequency variation due the temperature variation inside the cavity is: $\Delta f / \Delta T = 187$ MHz/K, or similarly 1 Hz per 5 nK.

These calculations show that without pressure control of the cavity, the frequency drift associated to the change of refractive index casued by temperature variationsis larger than the drift associated to the thermal expansion of the cavity. For now, the temperature controller used in this experiment is not precise enough to temperature stabilise the cavity at this level.

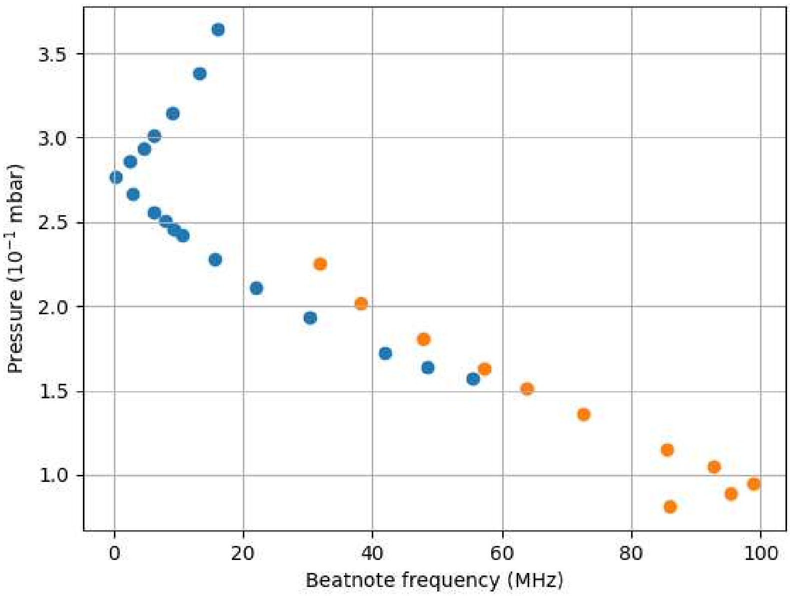

Figure 4.20: Evolution of the beat note frequency after pumping the ULE cavity down to $7 \cdot 10^{-2}$ mbar. This plot shows the drift of the beat note right after the pumps were turned off. These measurements were taken over the course of around 2 hours. The pressure reading is not directly taken on the ULE vacuum cavity so the actual pressure of the ULE is probably higher than these values. The frequency values stay between 0 and 100 MHz because the repetition frequency of the frequency comb is of 200 MHz. The ECDL is beating with one tooth of the comb, and then because of such high drift, it will beat with the next tooth. This explains the behaviour of the beat note frequency around 0 and 100 MHz.

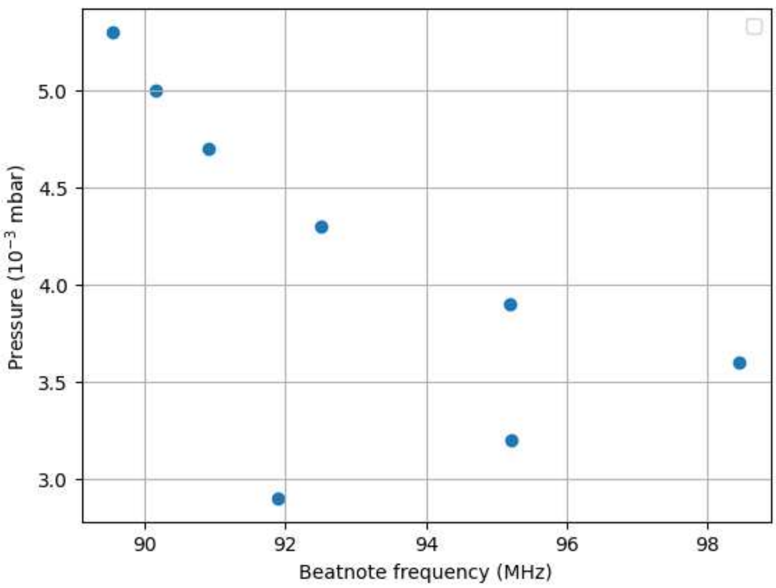

Figure 4.21: Evolution of the beat note frequency when the temperature controlled ULE cavity is continuously pumped. We see the same behaviour around 100 MHz as in Figure 4.20 for the same reasons.

5 Conclusion and perspectives

During this master's thesis, the assembly, characterisation and frequency stabilisation of a 1550 nm ECDL has been successfully achieved. This ECDL has been used in various optical cavity locking configurations, and successfully locked to cavities of varying finesse. Locking the ECDL to these cavities has improved its frequency stability by reducing the drift observed in the free-running laser. For the high-finesse cavity, a significant narrowing of the ECDL linewidth was observed, from approximately 100 kHz down to probably less than 1 kHz. This demonstrates that home-built ECDLs can be locked to very high-finesse optical cavities, reducing their linewidth considerably. Additionally, this work shows that the ECDL can stay locked for a few hours to a cavity made of Ultra Low Expansion (ULE) glass.

As it was explained in this work, the ECDL is currently in a box and on rubber holder to isolate it from its environment. This isolation can be improved by suspending the ECDL either with springs or with a pendulum-like type of mechanism, as the ECDL still unlocks when the table is touched. To stabilise the ECDL even more, a temperature control system can be placed inside the isolation box, as well as a pressure controller. The ECDL is sensitive to pressure change in the room; when the door is opened, the beat note drifts and if the laser is locked, it unlocks duethe resulting pressure variation. Pressure controlling the isolation box would suppress these effects and the ECDL could stayed locked for an even longer time.

To further develop a stable oscillator, the ULE cavity setup can be additionally optimised. Firstly, the finesse of this cavity can be increased, as it has been shown that locking to really high-finesse cavities is possible. To increase the cavity's finesse, its mirrors need to be changed. We are now looking into mirrors with a higher reflection coefficient and optimised radius of curvature to improve mode-matching between the beam and the cavity.
Something that has not really been explored in this thesis, but is quite interesting to look at, is the vacuum cavity setup. Currently, beam injection into the cavity is difficult because of the alignment screws of the fibre coupler holder, which are not precise enough. Furthermore, the distance between the output of the fibre and the input mirror of the cavity is fixed so it is restraining a lot the choices of lenses that can be used for a good mode-matching.
Something else concerning this cavity is the pump that has been used. This pump limits the level of vacuum that can be reached, so we are looking into another type of pump that could allow to go at least to 10^{-8} mbar, which would potentially reduce or eliminate the pressure associated drift of the beatnote. The drift rate can also be reduced with the temperature stabilisation of the ULE cavity. We can look more into the zero-crossing of the ULE, the temperature at which its thermal expansion coef-

ficient is 0, and develop a system allowing to stabilise the cavity at this temperature.

Moreover, the measurement of the linewidth of the ECDL can be improved by using a self-heterodyning technique, for example. This technique, developed by Okoshi [50], consists of splitting the laser beam and combining the two parts of the beam, with one having travelled through a very long fibre and being time delayed. The beatnote used in this method represents the beating of the laser with itself, allowing to measure accurately its linewidth because the beat note width would be exactly twice the laser's width. With this technique, there is no limitation due to the reference's linewidth because the reference is the laser in itself.
Another technique would be to beat the ECDL's with a laser that we know precisely the linewidth of, preferably in the kHz range.
The β-separation line method can be improved by introducing an intensity stabilisation loop in the setup, to remove unwanted noise from the transmission signal. This would therefore improve the precision of the linewidth values calculated with this method.

We are also limited by the available time window of our oscilloscope for the Allan deviation measurements. Because of this limitation, we cannot have a good idea of the stability of our oscillator over a long time period, which is crucial in optical clock development. The data acquisition of the time trace could be automated, allowing to have multiple traces of the same duration. These traces could then be piled up to make a longer time trace, which would allow to measure the stability of the oscillator for a longer time period.

All of these improvements could lead to the assembling of a precise and stable frequency reference here at UCLouvain.

A Appendix

A.1 Allan deviation validation

Calculating the Allan deviation can be quite challenging. For this work, the allantools library in Python was used, specifically the *oadev* function. This function takes as input either the phase or the frequency of the measured signal. In this work, the phase and frequency were computed by performing a Hilbert transform on the signal, calculating the instantaneous phase, and then differentiating this phase to obtain the instantaneous frequency.
The instantaneous frequency is then normalised by the ECDL frequency to obtain a unitless value, as the *oadev* function requires either phase or fractional frequency as input [51].

The Allan deviation plot obtained with this library was compared to a plot derived with the analytic function expressed in Equation 2.17. Both plots were found to be identical, confirming the accuracy of the allantools library.

Afterwards, these plots were compared with a simulated signal to verify if the obtained results were reliable. In this simulation, a signal was created with a carrier frequency of 40 MHz and a relative frequency variation of $3 \cdot 10^{-7}$. These values were chosen to replicate the measured beat frequency and to match the first point on the previously calculated Allan deviation plots. Fluctuations in the signal were then introduced to simulate white frequency noise. Finally, the noisy signal was normalised by the carrier frequency, and its Allan deviation was calculated. The result of this simulated signal is shown in Figure A.1. As can be seen on this figure, the measured Allan deviation closely matches the simulated one, which helps validating the accuracy of our method.

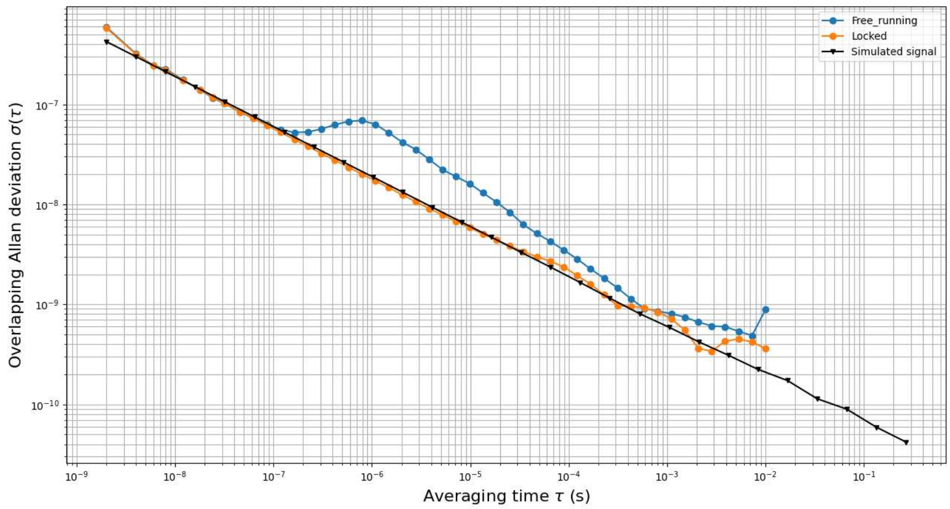

Figure A.1: Overlapping Allan deviation of the free-running ECDL in blue, the locked ECDL to the ULE cavity in orange and a simulated time signal affected by only white frequency noise in black.

Bibliography

[1] Bureau International des Poids et Mesures (BIPM), *The International System of Units (SI), 9th Edition.* Sèvres, France: Bureau International des Poids et Mesures, 2019, accessed: 2025-05-12. [Online]. Available: https://www.bipm.org/documents/20126/41483022/SI-Brochure-9.pdf/fcf090b2-04e6-88cc-1149-c3e029ad8232

[2] P. Maddaloni, M. Bellini, and P. D. Natale, *Laser-Based Measurements for Time and Frequency Domain Applications: A Handbook.* Boca Raton, FL, USA: CRC Press, 2016.

[3] M. A. Lombardi, "The accuracy and stability of quartz watches," *Horological Journal*, vol. 150, no. 2, pp. 57–59, 2008. [Online]. Available: https://www.nist.gov/publications/accuracy-and-stability-quartz-watches

[4] National Institute of Standards and Technology, "Nist's cesium fountain atomic clocks," https://www.nist.gov/pml/time-and-frequency-division/time-realization/cesium-fountain-atomic-clocks, 2023, accessed: 2025-06-02. [Online]. Available: https://www.nist.gov/pml/time-and-frequency-division/time-realization/cesium-fountain-atomic-clocks

[5] T. E. Parker and J. Levine, "Impact of new high stability frequency standards on the performance of the nist at1 time scale," *IEEE Transactions on Ultrasonics, Ferroelectrics, and Frequency Control*, vol. 44, no. 6, pp. 1239–1244, 1997.

[6] T. L. Nicholson, M. J. Martin, J. R. Williams, B. J. Bloom, M. Bishof, M. D. Swallows, S. L. Campbell, and J. Ye, "Comparison of two independent sr optical clocks with 1×10^{-17} stability at 10^3 s," *Physical Review Letter*, vol. 109, no. 23, p. 230801, 2012.

[7] S. Häfner, . S. Falke, C. Grebing, S. Vog, T. Legero, M. Merimaa, C. Lisdat, and U. Sterr, "8×10^{-17} fractional laser frequency instability with a long room-temperature cavity," *Optics Letters*, vol. 40, no. 9, pp. 2112–2115, 2015.

[8] C. W. Chou, D. B. Hume, T. Rosenband, and D. J. Wineland, "Optical clocks and relativity," *Science*, vol. 329, no. 5999, pp. 1630–1633, 2010.

[9] T. Bothwell, C. J. Kennedy, A. Aeppli, D. Kedar, J. M. Robinson, E. Oelker, A. Staron, and J. Ye, "Resolving the gravitational redshift across a millimetre-scale atomic sample," *Nature*, vol. 602, no. 7897, pp. 420–424, 2022.

[10] M. D. Álvarez, *Optical Cavities for Optical Atomic Clocks, Atom Interferometry and Gravitational-Wave Detection*, 1st ed., ser. Springer Theses. Springer International Publishing, 2019.

[11] I. Bayrakli, "Frequency stabilization at the sub-kilohertz level of an external cavity diode laser," *Applied Optics*, 2016, suleyman Demirel University, Biomedical Engineering, Turkey.

[12] B. Dahmani, L. Hollberg, and R. Drullinger, "Frequency stabilization of semiconductor lasers by resonant optical feedback," *Optics Letters*, vol. 12, no. 11, pp. 876–878, Nov 1987, received: May 20, 1987; Accepted: August 12, 1987.

[13] Y. Zhao, Y. Li, Q. Wang, F. Meng, Y. Lin, S. Wang, B. Lin, S. Cao, J. Cao, Z. Fang, T. Li, and E. Zang, "100-hz linewidth diode laser with external optical feedback," *IEEE Photonics Technology Letters*, vol. 24, no. 20, pp. 1795–1798, Oct 2012.

[14] S. Hirata, T. Akatsuka, Y. Ohtake, and A. Morinaga, "Sub-hertz-linewidth diode laser stabilized to an ultralow-drift high-finesse optical cavity," *Applied Physics Express*, vol. 7, no. 2, p. 022705, 2014, received: December 11, 2013; Accepted: January 13, 2014; Published: January 30, 2014.

[15] S. Peil, W. Tobias, J. Whalen, B. Hemingway, and T. G. Akin, "Progress on optical clock technology for operational timescales," in *9th Symposium on Frequency Standards and Metrology*, vol. 2889, no. 1. IOP Publishing, 2024, pp. 1–6.

[16] S. C. Doret, "Simple, low-noise piezo driver with feed-forward for broad tuning of external cavity diode lasers," *Review of Scientific Instruments*, vol. 89, no. 2, p. 023102, 2018.

[17] C. hua Wei, C. lin Zuo, L. Liang, and S. hua Yan, "Compact external cavity diode laser for quantum experiments," *Optoelectronics Letters*, vol. 16, no. 6, pp. 393–397, November 2020, received 12 February 2020; Revised 31 March 2020.

[18] G.-Z. Pan, B.-L. Guan, C. Xu, P.-T. Li, J.-W. Yang, and Z.-Y. Liu, "Broad bandwidth interference filter-stabilized external cavity diode laser with narrow linewidth below 100 khz," *Chinese Physics B*, vol. 27, no. 1, p. 014204, 2018, published online 28 November 2017; Received 10 July 2017; Revised 14 August 2017.

[19] B. Han, Y. Shi, X. Tang, J. Li, C. Guan, J. Ye, and R. Shen, "Precisely tunable 780 nm external cavity diode laser," *Photonics*, vol. 12, no. 4, p. 293, 2025, received: 9 February 2025; Revised: 25 February 2025; Accepted: 18 March 2025; Published: 21 March 2025.

[20] D. J. Thompson and R. E. Scholten, "Narrow linewidth tunable external cavity diode laser using wide bandwidth filter," *Review of Scientific Instruments*, vol. 83, no. 2, p. 023107, 2012, received: 7 August 2011; Accepted: 2 February 2012; Published: 24 February 2012.

[21] S. Bennetts, G. D. McDonald, K. S. Hardman, J. E. Debs, C. C. N. Kuhn, J. D. Close, and N. P. Robins, "External cavity diode lasers with 5khz linewidth and 200nm tuning range at 1.55µm and methods for linewidth measurement," *Optics Express*, vol. 22, no. 9, pp. 10 642–10 654, 2014.

[22] L. Ricci, M. Weidemüller, T. Esslinger, A. Hemmerich, C. Zimmermann, V. Vuletić, W. König, and T. W. Hänsch, "A compact grating-stabilized diode laser system for atomic physics," *Optics Communications*, vol. 117, no. 5-6, pp. 541–549, June 1995, received: 21 December 1994.

[23] R. W. P. Drever, J. L. Hall, F. V. Kowalski, J. Hough, G. M. Ford, A. J. Munley, and H. Ward, "Laser phase and frequency stabilization using an optical resonator," *Applied Physics B*, vol. 31, pp. 97–105, 1983.

[24] D. Kedar, Z. Yao, I. Ryger, J. L. Hall, and J. Ye, "Synthetic fm triplet for am-free precision laser stabilization and spectroscopy," *Optica*, vol. 11, no. 1, pp. 58–63, January 2024, received 6 October 2023; revised 23 November 2023; accepted 24 November 2023; published 9 January 2024.

[25] E. D. Black, "An introduction to pound–drever–hall laser frequency stabilization," *American Journal of Physics*, vol. 69, no. 1, pp. 79–87, 2001, lIGO Project, California Institute of Technology, Mail Code 264-33, Pasadena, California 91125.

[26] G. Ruoso, R. Storz, S. Seel, S. Schiller, and J. Mlynek, "Nd:yag laser frequency stabilization to a supercavity at the 0.1 hz level," *Optics Communications*, vol. 133, no. 1–6, pp. 259–262, January 1997, received 6 March 1996; Accepted 5 June 1996.

[27] Q.-F. Chen, A. Nevsky, and S. Schiller, "Locking the frequency of lasers to an optical cavity at the 1.6×10^{-17} relative instability level," *Applied Physics B*, 2012, published online; Received: 17 January 2012; Revised: 26 March 2012.

[28] J. Langbein, "Estimating rate uncertainty with maximum likelihood: differences between power-law and flicker–random-walk models," *Journal of Geodesy*, vol. 86, no. 10, pp. 775–783, 2012.

[29] F. Riehle, *Frequency Standards: Basics and Applications*. Weinheim, Germany: Wiley-VCH, 2004, ch. 3, chapter 3.

[30] N. Picqué and T. W. Hänsch, "Frequency comb spectroscopy," *Nature Photonics*, vol. 13, pp. 146–157, 2019.

[31] C. Lauzin, "How to measure a wavelength, a frequency, the question of accuracy," Lecture slides, LPHYS22246 - Experimental methods in atomic and molecular physics, 2024, accessed: 2025-06-02.

[32] J.-Q. Chen, C. Chen, J.-J. Sun, J.-W. Zhang, Z.-H. Liu, L. Qin, Y.-Q. Ning, and L.-J. Wang, "Linewidth measurement of a narrow-linewidth laser: Principles, methods, and systems," *Sensors*, vol. 24, no. 11, p. 3656, 2024.

[33] M. Chen, Z. Meng, J. Wang, and W. Chen, "Ultra-narrow linewidth measurement based on voigt profile fitting," *Optics Express*, vol. 23, no. 5, p. 6803, 2015, received 15 Jan 2015; revised 2 Mar 2015; accepted 2 Mar 2015; published 4 Mar 2015.

[34] J. J. Olivero and R. L. Longbothum, "Empirical fits to the voigt line width: A brief review," *Journal of Quantitative Spectroscopy and Radiative Transfer*, vol. 17, pp. 233–236, 1977, ionosphere Research Laboratory, The Pennsylvania State University, University Park, PA 16802, U.S.A.

[35] L. B. Mercer, "$1/f$ frequency noise effects on self-heterodyne linewidth measurements," *Journal of Lightwave Technology*, vol. 9, no. 4, pp. 485–493, April 1991.

[36] G. M. Stéphan, T. T. Tam, S. Blin, P. Besnard, and M. Têtu, "Laser line shape and spectral density of frequency noise," *Physical Review A*, vol. 71, p. 043809, 2005, received: 30 June 2004; Published: 11 April 2005.

[37] C. H. Henry, "Theory of the linewidth of semiconductor lasers," *IEEE Journal of Quantum Electronics*, vol. QE-18, no. 2, pp. 259–264, February 1982.

[38] G. D. Domenico, S. Schilt, and P. Thomann, "Simple approach to the relation between laser frequency noise and laser line shape," *Applied Optics*, vol. 49, no. 25, pp. 4801–4807, 2010, this citation should be used for any reference to this work.

[39] D. W. Allan, "Statistics of atomic frequency standards," *Proceedings of the IEEE*, vol. 54, no. 2, pp. 221–230, February 1966.

[40] C. Goueguel, "Laser linewidth, phase noise, frequency noise, and all that," https://christiangoueguel.github.io/blog/posts/post10/index.html, 2024, accessed: 2025-05-26.

[41] T. V. Baak, "The fury of the time nut," http://www.leapsecond.com/pages/fury/, 2005, accessed: 2025-05-26.

[42] Tektronix, *Fundamentals of Real-Time Spectrum Analysis*, https://download.tek.com/document/37W_17249_6_Fundamentals_of_Real-Time_Spectrum_Analysis1.pdf, 2014, accessed: 2025-06-02.

[43] MOG Laboratories Pty Ltd, *MOGLabs FSC100 Fast Servo Controller Manual*, MOG Laboratories Pty Ltd, 2019, version 0.1.2, Rev 2–4 hardware. [Online]. Available: https://www.manualslib.com/manual/1920303/Moglabs-Fsc100.html

[44] R. Glorieux, "High-resolution spectroscopic investigation of the systematic increase of vibrational excitation in water-containing van der waals complexes," Ph.D. thesis, Faculté des sciences, UCLouvain, Louvain-la-Neuve, Belgium, December 2023.

[45] S. T. Gulati and M. J. Edwards, "Uletm - zero expansion, low density, and dimensionally stable material for lightweight optical systems," in *Proceedings*

of SPIE - Advanced Materials for Optics and Precision Structures, vol. CR67. San Diego, CA, USA: SPIE, 1997, pp. 107–136.

[46] D. W. Allan and J. Levine, "A historical perspective on the development of the allan variances and their strengths and weaknesses," *IEEE Transactions on Ultrasonics, Ferroelectrics, and Frequency Control*, vol. 63, no. 4, pp. 513–519, April 2016.

[47] P. E. Ciddor, "Refractive index of air: new equations for the visible and near infrared," *Applied Optics*, vol. 35, no. 9, pp. 1566–1573, 1996.

[48] M. Lachance, M. Séguin, , B. Villeneuve, and B. Marcheterre, *Physique mécanique 1*, 5th ed. Bruxelles, Belgique: De Boeck Supérieur, 2015, ch. 16, adaptation française de l'ouvrage de Benson.

[49] NIST, "Ciddor refractive index of air calculator," https://emtoolbox.nist.gov/Wavelength/Ciddor.asp, 2025, accessed: 2025-05-26.

[50] T. Okoshi, K. Kikuchi, and A. Nakayama, "Novel method for high resolution measurement of laser output spectrum," *Electronics Letters*, vol. 16, no. 16, pp. 630–631, 1980.

[51] AllanTools Contributors, "Allantools: `oadev()` function documentation," https://allantools.readthedocs.io/en/latest/functions.html#allantools.oadev, 2025, accessed: 2025-05-26.

The redaction of this master's thesis was helped by ChatGPT for checking spelling, grammar, and sentence construction.

UNIVERSITE CATHOLIQUE DE LOUVAIN

Faculté des sciences

Place des sciences, 2 bte L6.06.01, 1348 Louvain-la-Neuve, Belgique | **www.uclouvain.be/sc**